Genome-wide CRISPR screen identifies KEAP1 as a genetic dependency of ARID1A-deficient cells

Fournier, LA[1,2]; Kalantari, F[3,4]; Wells, JP.[1]; Lee, JS[5]; Trigo-Gonzalez, G[4]; Moksa, MM[5]; Smith, T[1]; White, J[1,6]; Shanks, A[1]; Wang, L[5]; Su, E[5]; Wang, Y[3,4]; Huntsman, DG[3,4,7]; Hirst, M[5,8]; and Stirling, PC[1,6,*]

[1] Terry Fox Laboratory, BC Cancer, Vancouver, BC, Canada
[2] Interdisciplinary Oncology Program, University of British Columbia, Vancouver, BC, Canada
[3] Department of Pathology and Laboratory Medicine, University of British Columbia, Vancouver, BC, Canada
[4] Department of Molecular Oncology, BC Cancer Research Centre, Vancouver, BC, Canada.
[5] Michael Smith Laboratories, University of British Columbia, Vancouver, BC
[6] Department of Medical Genetics, University of British Columbia, Vancouver, BC
[7] Department of Obstetrics and Gynaecology, University of British Columbia, Vancouver, BC, Canada.
[8] Genome Sciences and Technology Program, University of British Columbia, Vancouver, BC, Canada.
[*] Correspondence to P.C.S.: pstirling@bccrc.ca

ABSTRACT

ARID1A is the core DNA binding subunit of the BAF chromatin remodeling complex and is mutated in about ~8% of all cancers. The frequency of ARID1A loss varies between cancer subtypes, with clear cell ovarian carcinoma (CCOC) presenting the highest incidence at >50% of cases. Despite a growing understanding of the consequences of ARID1A-loss in cancer, there remains limited targeted therapeutic options for ARID1A-deficient cancers. Using a genome-wide CRISPR screening approach, we identify KEAP1 as a synthetic lethal partner of ARID1A in CCOC. Depletion or chemical inhibition of KEAP1 results in the selective killing of ARID1A-KO cells. While we confirm that KEAP1-NRF2 signalling is dysregulated in ARID1A-KO cells, we suggest that this synthetic lethality is not due to aberrant NRF2 signalling. Rather, we find that KEAP1 perturbation exacerbates genome instability phenotypes associated with ARID1A-deficiency. We also confirm the selective killing of ARID1A-KO cells by the KEAP1 inhibitor AI-1 in edited primary endometrial epithelial cells and organoids. Together, our findings uncover a novel therapeutic avenue for the treatment of cancers harboring ARID1A mutations.

KEY WORDS: Synthetic lethality, ARID1A, KEAP1, CRISPR screening

AUTHOR SUMMARY

ARID1A, a component of a protein complex that regulates DNA accessibility, is frequently mutated in various cancers. Ovarian clear cell carcinoma (CCOC) is particularly affected, with over 50% of cases showing ARID1A loss. Despite growing knowledge on ARID1A loss in cancer, therapeutic options for ARID1A-deficient tumors remain limited. Using high throughput CRISPR screening, we identified KEAP1 perturbation as a sensitivity of ARID1A-deficient cells in cell lines and patient-derived samples. While the exact mechanism underlying this sensitivity remains uncertain, we showed that perturbation of KEAP1 exacerbates the heightened DNA damage states associated with ARID1A-deficiency. Taking advantage of these findings, we showed that combination treatment against KEAP1 and the DNA repair protein ATR results in improved killing of ARID1A-depleted cancer cells. Ultimately, our results provide new knowledge on the consequences of ARID1A loss in cancer and suggest that KEAP1 inhibition may provide clinical benefit to selectively eliminate ARID1A-deficient tumours.

INTRODUCTION

AT-rich interaction domain 1A (ARID1A) is the DNA binding subunit of the BAF complex, the canonical SWI/SNF chromatin remodeling complex, which regulates a variety of processes within the cell, including chromatin accessibility, gene expression and the maintenance of genome integrity. ARID1A is mutated in ~8% of all cancers, with clear cell ovarian carcinoma (CCOC) presenting the highest incidence of ARID1A loss at >50% of cases [1,2]. ARID1A mutations are typically missense or frameshift in nature, occur throughout the length of the gene, and result in loss of protein expression. While ARID1A loss has shown prognostic value for several neoplastic malignancies (e.g. gastric[3–5], lung[6], hepatocellular[7–9], breast[10], and renal carcinoma), it remains ambiguous how ARID1A status influences the prognosis of gynecologic malignancies. Previous studies have reported adverse clinical outcomes for patients harbouring ARID1A mutations[10,11], though conflicting reports have emerged suggesting no clinical association (e.g. stage, survival and histopathological features) between ARID1A-positive and negative cohorts[12–17]. Nevertheless, loss of ARID1A is widely recognized as an enabling factor for cancer development and progression.

ARID1A deficiency results in a broad range of phenotypes, including genome instability[18–20], transcriptional dysregulation[21,22], and metabolic dysfunction[23–25]. Despite an increasing body of evidence documenting context-specific consequences of ARID1A loss in cancer, there remains a critical gap in knowledge as to how to selectively treat patients harboring these lesions. Genetic dependencies of ARID1A have been used to suggest novel therapeutic avenues against ARID1A-deficient cancer cells. For example, taking advantage of the antagonistic relationship between BAF and the polycomb repressive 2 (PRC2) complex on the regulation of gene expression[26–28], the EZH2 inhibitor tazemetostat is currently in phase II clinical trials for the treatment of ARID1A-deficient ovarian cancers[29–31] (EPZ-IST-001). Other promising therapies include BET inhibitors (e.g. JQ1)[32], agents targeting DNA or replication stress responses (ATR/PARP inhibitors)[18], and aurora kinase A (AURKA) inhibitors[33]. The diverse targets of these inhibitors reflect the diversity of cellular activities disrupted by ARID1A loss.

In this study we use a genome-wide CRISPR screening approach to identify genes important for fitness in an isogenic CCOC cell line model of ARID1A loss. We identify the oxidative stress regulator KEAP1 as a novel synthetic lethal partner of ARID1A. We document that ARID1A-KO cells are sensitive to KEAP1 perturbation with CRISPR, small molecule inhibitors and RNAi, resulting in enhanced genome instability and DNA replication stress phenotypes. Building on these findings, we show that the combination treatment of ATR inhibitors and KEAP1 inhibitors results in enhanced killing of ARID1A-KO cells, supporting the idea that the genome instability induced in ARID1A-KO following KEAP1 inhibiting can be harnessed therapeutically. While we observed a general dysregulation of KEAP1-NRF2 signalling in ARID1A-KO cells in clinical and cell line samples, knockdown of NRF2 did not rescue the sensitivity of ARID1A-KO cells to KEAP1 inhibition. We suggest that perhaps other functions of KEAP1 underlie the genetic dependency between KEAP1 and ARID1A. Finally, we extend the potential clinical relevance of this genetic dependency in patient-derived models. Altogether, our findings uncover a novel therapeutic avenue for the selective killing of ARID1A-deficient CCOC.

RESULTS

Genome-wide CRISPR screen identifies genes important for fitness in ARID1A-KO CCOC cells

To identify genes important for fitness when ARID1A is lost in the context of CCOC, we performed genome-wide CRISPR screens in biological duplicates in RMG-1 cells and its ARID1A knockout (ARID1A-KO) derivative using the Toronto Knockout version 3 library (TKOv3)[34] (**Fig 1A**). RMG-1 ARID1A-KO cells were generated using CRISPR as documented previously[19] (**Fig S1A**). Cells were infected at >500X coverage of the library and were cultured until 14 days post puromycin selection to capture robust fitness defects induced by sgRNA knockouts. Genomic DNA was purified and sgRNA representation was assessed by deep amplicon sequencing (>99% sgRNA representation across all samples). Reads were aligned to the TKOv3 library using Bowtie2[35] and sgRNA enrichment was calculated using the BAGEL2 pipeline[36], which integrates the fitness scores from all four sgRNAs into a single value for each target gene. Bayes Factor (BF) scores obtained from the BAGEL2 analysis were compared between the ARID1A-WT and ARID1A-KO datasets to identify genes important for fitness, specifically within the ARID1A-KO populations. As expected, non-targeting control sgRNAs targeting eGFP, LacZ and Luciferase presented to lowest BF scores (**Table S1**) across all samples. Furthermore, our approach recovered >87.5% of the training dataset of core essential genes (CEGs) as important for fitness across our samples (**Table S1B-C**). As further validation to our experimental approach, precision-recall (PR) curves were plotted to assess screen performance, and the high precision-to-recall ratio suggested a low false positive (precision) and high false-negative rates (recall) (**Fig 1B**).

In total, each biological replicate of our screen identified a consensus of 1,484 genes important for fitness of ARID1A-KO cells (**Supplemental Table 1.7**). To investigate the potential functional repertoire of all the identified hits, we performed a GO analysis on this dataset, which revealed an enrichment in pathways relating to gene expression, cell cycle and mitochondrial function, which agrees with the literature on ARID1A-deficiency in cancer[37–40] (**Fig 1D and Table S2.1**). To focus on potential genetic dependencies unique to ARID1A-KO cells,

we filtered out fitness genes that were also identified in ARID1A-WT cells. This resulted in 881 and 699 ARID1A-KO-specific hits from each replicate, with a significant overlapping consensus of 103 high-confidence synthetic lethal partners, dubbed "ARID1A-SL" ($p < 5.588e-26$, hypergeometric test, **Fig 1C and Table S1.8** and **S2.2**). Importantly, the overlap of 103 genes successfully identifies known ARID1A synthetic lethal partners in DDX19A[41], SMARCC1[42], and FAAP24[41] amongst others (**Table S1.8**). Additional known synthetic lethal partners were also recovered in either of the screen replicates (e.g. SMARCB1/E1[42], ARID1B[43], and BRD2[32]; **Table S1.8**).

To prioritize and pursue strong novel candidate synthetic lethal partners of ARID1A for further validation, we averaged the BF score of the ARID1A-SL dataset and ranked the top hits (**Fig 1E**). This approach identified PNPO, CTDSP1 and KEAP1 as the top essential genes when ARID1A is lost. PNPO encodes pyridoxine 5'-phosphate oxidase, which converts dietary vitamin B6 into its biologically active form, contributing to a variety of metabolic processes. CTDSP1 encodes a small phosphatase that targets serine 5 in the heptameric repeats of the C-terminal domain of the large RNA polymerase II subunit POLR2A, controlling gene expression dynamics for most PolII genes. PNPO and CTDSP1 are interesting hits, but likely have pleiotropic effects on global cellularly phenomena. KEAP1 on the other hand is a ubiquitin E3 ligase whose major target, NRF2, a transcription factor with roles in the regulation of metabolism, inflammation, mitochondrial function and more[44]. NRF2's activity is tightly regulated by KEAP1 under normal conditions, whereby KEAP1 sequesters NRF2 and targets it for proteasomal degradation. We further assessed the validity of KEAP1 as a hit by looking at the normalized read counts for all 4 sgRNAs and confirmed the dropout of these guides in the ARID1A-KO samples (**Figure S1F**). Given these data, the fact that ARID1A physically interacts with NRF2, and that the disruption of this interaction results in fitness defects[24], we chose to focus on validating KEAP1 as a synthetic lethal partner of ARID1A in CCOC.

Validation of KEAP1 as a synthetic lethal partner of ARID1A

To validate the potential synthetic lethal relationship between ARID1A and KEAP1, we generated an additional isogenic cell line model of ARID1A loss in RPE1-hTERT cells, which we validated with western blot and sanger sequencing (**Fig S1D-E**). RPE1-hTERT is a retinal epithelial cell line that is immortalized by hTERT expression but non-transformed and was chosen to represent a very different cell context compared to RMG-1. We independently transfected our ARID1A isogenic cell line pairs (i.e., from RMG-1 or RPE1 parental lines) with two independent siRNAs targeting KEAP1, and performed a viability assay with crystal violet staining to assess the sensitivity of ARID1A-KO cells to KEAP1 depletion. ARID1A-KO cells showed decreased survival following KEAP1 knockdown when compared to their ARID1A-WT parental cells in both cellular backgrounds, as measured by the decrease in crystal violet staining (**Fig 2A-B** and **Fig S2A**). As expected, knockdown of KEAP1 resulted in decreased KEAP1 protein expression that was accompanied by an increase in the levels of its major target protein, NRF2 (**Fig S2B-C)**.

In a parallel approach, we treated ARID1A-deficient or proficient pairs of RMG-1 and RPE1 cells with the small molecule inhibitors of KEAP1, AI-1 and L-sulforaphane (SFN), both of

which covalently modifying cysteine residues on KEAP1's C-terminus to release of NRF2 from KEAP1 inhibition[45,46]. ARID1A-KO cells showed sensitivity to AI-1 in both models when compared to their ARID1A-WT counterparts (**Fig 2C-D)**. While ARID1A-KO cells exhibited growth defects under KEAP1 inhibition by SFN in the RPE1 background (**Fig 2E**), we did not observe significant growth defects in the RMG-1 cells (**Fig S2D**). As expected, treatment with AI-1 and SFN both resulted in an induction of NRF2 protein levels (**Fig S2E**). To further test the potential generalizability of these findings, we assessed the toxicity of AI-1 on a panel of CCOC cell lines grouped by ARID1A status and observed a trend in which ARID1A-mutated cells presented lower IC50 values compared to the WT counterparts (**Fig 2F** and **Fig S2F-G**). Altogether these results confirm the observations from our CRISPR screen and suggest that KEAP1 is a synthetic lethal partner of ARID1A.

Differential gene expression analysis reveals dysregulation of NRF2 target genes in ARID1A-KO cells

To gain further insight on the potential mechanism underlying the synthetic lethality between KEAP1 and ARID1A, we first assessed if and how NRF2 signalling may be disrupted in ARID1A-KO cells. To do so, we revisited RNA-seq data from Wu *et al.*[22] in RMG-1 cells that either had intact or mutated ARID1A status[22]. Although this isogenic line was generated using different sgRNAs, these cells possess a similar genetic background as that used for our CRISPR screens. Differential gene expression (DGE) analysis using DESEQ2[47] revealed that ARID1A-loss incurred a significant up-regulation of 531 genes (ARID1A-UP), and down-regulation of 500 genes (ARID1A-DOWN) (**Fig 3A** and **Table S3**). GO analysis using the ENCODE and ChEA datasets on the differentially expressed genes revealed a significant enrichment of NRF2 (also NFE2L2) target genes (**Fig 3B**). These results highlight how ARID1A loss results in significant changes in NRF2-mediated gene expression, and perhaps support the notion that KEAP1 signalling may be disrupted in the cells.

To test this hypothesis, and since KEAP1 and ARID1A are commonly mutated in cancer[1,2,48], we compared mRNA expression of KEAP1 and ARID1A in a large cohort of solid tumours of various origins from The Cancer Genome Atlas (TCGA) datasets (**Fig 3C)**. This analysis revealed that transcript levels from KEAP1 inversely correlated with ARID1A, albeit mildly, across a pan-cancer panel ($n = 10{,}071$, $r = -0.12$, $p = 2.2e^{-16}$). This observation suggests that ARID1A and KEAP1 perhaps compensate for the loss of each other in cancer development. Furthermore, stratification of patients by ARID1A mutational status confirmed this relationship, where some ARID1A-mutated cancer subtypes (e.g. stomach adenocarcinoma - "stad") appear to upregulate KEAP1 compared to wild-type (**Fig 3D** and **Fig S3A**). As further support to this notion, we quantified KEAP1 protein levels from western blots and found a small but significant increase in KEAP1 protein levels in ARID1A-KO cells compared to wild-type (**Fig 3E**). Overall, our data suggests that ARID1A-deficient cells upregulate KEAP1, perhaps as a defense mechanism to prevent fitness defects and promote cancer.

Aberrant NRF2 signalling cannot explain ARID1A-KEAP1 synthetic lethality

To explore the possibility that aberrant NRF2 signalling may explain the synthetic lethal relationship between KEAP1 and ARID1A, we generated mutant NRF2-inducible cell lines by

transducing our isogenic RMG-1 model (+/- ARID1A) with lentiviral particles containing a pIND20-NRF2^{E79Q}-HA construct. The E79Q mutation in NRF2 confers reduced binding affinity for KEAP1, resulting in an NRF2 protein that cannot be inhibited by KEAP1 and is constitutively active [49]. When we induced the expression of the NRF2^{E79Q} protein in our ARID1A-WT and KO cells using doxycycline, we observed a very minor reduction in survival of ARID1A-KO cells but not WT cells (**Fig 3F** and **Fig S3B-C**). This phenotype was restricted to the highest dosage of doxycycline (2µg/mL), and we observed no sensitivity to doxycycline at the doses tested (**Fig S3D**). Our data therefore suggests that perhaps the dysregulation of the KEAP1 signalling as a whole, and not NRF2 itself, may be responsible for the sensitivity displayed by ARID1A-KO cells.

In order to gain a deeper understanding of the mechanism of synthetic lethality underlying the dependency between KEAP1 and ARID1A, we sought to determine if NRF2 signaling, downstream of KEAP1, could explain the sensitivity of ARID1A-deficient cells to AI-1. To do so, we knocked down NRF2 using siRNA and assessed cell growth after 60 hours of AI-1 treatment (**Fig S3E**). Interestingly, while AI-1 treatment induced NRF2 protein expression (**Fig S3F**), knockdown of NRF2 did not rescue the growth defects observed in ARID1A-KO cells after 60 hours of treatment with AI-1 (**Fig 3G**), suggesting that KEAP1 inhibition-mediated growth suppression of ARID1A-KO cells is independent of NRF2 activation. As expected, knockdown of KEAP1 caused significant growth defects in the KO but not the WT cells. Surprisingly however, dual knockdown of KEAP1 and NRF2 resulted in more significant growth defects in ARID1A-KO cells, supporting the notion that additional roles of KEAP1 may account for the sensitivity observed in ARID1A-KO cells. Furthermore, while AI-1 has been suggested to have potential off-target effects on histone deacetylase 1 (HDAC1), we did not observe major changes in protein levels at the doses tested (**Fig S3F**). Overall, our results suggest that NRF2 dysregulation is unlikely to fully account for the toxicity of KEAP1 perturbation in ARID1A-KO cells.

KEAP1 perturbation exacerbates genome instability in ARID1A-deficient cells

Since the canonical KEAP1 substrate NRF2 does not seem to explain the observed synthetic lethality with ARID1A loss, we sought other explanations. Our group has previously reported that ARID1A-deficient cells experience increased rates of DNA replication stress and DNA damage[19]. To assess whether the sensitivity of ARID1A-KO cells to KEAP1 inhibition could be associated with genome instability phenotypes, we performed immunofluorescence assays to measure p-RPA(ser33) foci formation. p-RPA(ser33) foci are thought to be a *bona fide* marker of DNA replication stress as they indicated RPA filaments modified by ATR. As expected, ARID1A-KO cells presented a higher accumulation of p-RPA(ser33) foci compared to WT cells (**Fig 4A**). Importantly, we observed a significant increase in DNA replication stress ARID1A-KO cells treated with sublethal doses of AI-1 (50µM), but not in ARID1A-WT cells. We observed a similar relationship in our RPE1 isogenic cell line model, where AI-1 treatment induced pRPA(ser33) foci formation in both the ARID1A-WT and KO cells, though the increase in KO cells was stronger (and **Fig S4A**). These results suggest that KEAP1 inhibition may enhance the genome instability phenotypes associated with ARID1A-loss.

To assess if the replication stress associated with KEAP1 inhibition also resulted in DNA damage, we performed an immunofluorescence assay probing for γH2AX foci formation. In

agreement with our previous results, we observed a significant increase in γH2AX foci formation in our RMG-1 ARID1A-KO cells (**Fig 4B**). As for our DNA replication stress phenotypes, 50μM AI-1 treatment caused a significant increase in γH2AX foci formation specifically in the ARID1A-KO cells, but not the WT. Similar phenotypes were observed in the RPE1 isogenic cell line: while AI-1 treatment caused a significant increase in γH2AX foci in the RPE1 ARID1A-WT cells compared to the DMSO control, ARID1A-KO cells accumulated more foci (**Fig S4B**). These data suggest that ARID1A and KEAP1 work in parallel to suppress DNA damage.

We also assessed genome instability phenotypes in ARID1A-WT and KO cells subjected to siRNA depletion of KEAP1. Consistent with previous results, ARID1A-KO cells presented higher levels of p-RPAser33 and γH2AX foci compared to WT under control conditions (**Fig S4C-D**). Additional knockdown of KEAP1 by siRNA did not result in a significant increase in p-RPAser33 and γH2AX foci in the RMG-1 derived cells (**Supplemental Fig 4C-D**), but did significantly enhance p-RPAser33 and γH2AX foci formation in our RPE1 cell line pair (**Fig S4E-F**). The reasons for the difference in penetrance of siRNA phenotypes in the two cell line pairs are unclear. However, further analysis by western blot suggested that RMG-1 ARID1A-KO cells, but not WT, present minor increases in the DNA replication stress markers p-RPA(ser33), p-ATR(428), and p-CHK1(345) following depletion of KEAP1 by siRNA (**Fig 4C**). Overall, our data suggests that perturbation of KEAP1 by chemical or siRNA means can exacerbate the genome instability phenotypes of ARID1A-KO cells.

If DNA damage and replication stress are to impact fitness, evidence of induced genome instability should be evident upon KEAP1 depletion. To test this, we assessed micronuclei formation by DAPI staining of the various treatment conditions outlined above. Micronuclei are typically formed due to lagging chromosomes during mitosis or appear in senescent cells due to a defective nuclear envelope[50]. We found that as reported, under normal conditions, ARID1A-KO cells present a higher frequency of micronuclei[20] (**Fig 4D**). Consistent with unresolved DNA replication stress measured above (i.e. p-RPA(ser33) and γH2AX increases), AI-1 treatment induced an increase in micronuclei formation specifically in ARID1A-KO cells, while no change could be observed in the ARID1A-WT cells. Furthermore, we measured a significant increase in micronuclei formation in ARID1A-KO RMG-1 cells subjected to siKEAP1, but not ARID1A-WT cells (**Fig 4E**). Similar phenotypes were also observed in our RPE1 isogenic cell line model (**Fig S4G-H**). Thus, we conclude that ARID1A-deficient cells exist in a sensitized state where KEAP1 inhibition with AI-1 or siRNA enhances genome instability phenotypes.

Dual inhibition of KEAP1 and ATR potentiates killing of ARID1A-KO cells

Since ARID1A-loss sensitizes cells to ATR inhibition[51], and we observed enhanced marks of replication stress when treating cells with KEAP1 inhibitors, we set out to test whether KEAP1 inhibition could potentiate the selective killing of these cells. To do so, we treated our isogenic RMG1 cells with sub-lethal concentrations of ceralasertib (CER), a potent ATR inhibitor, alone or in combination with AI-1 (**Fig 4F**). While neither AI-1 (75μM) nor CER (25nM) treatment alone resulted in significant killing of RMG-1 ARID1A-KO cells, the combination treatment of AI-1+CER resulted in the potentiation of the killing of ARID1A mutants (**Fig 4F**). This data agrees with the genome instability phenotypes induced by KEAP1 inhibition in ARID1A-KO cells and

suggests that combinations with ATRi could be harnessed to improve the selective killing of ARID1A-KO cells by KEAP1 inhibitors.

AI-1 treatment selectively kills primary endometrial epithelial cells deficient for ARID1A

Finally, to assess the clinical relevance of the ARID1A-KEAP1 synthetic lethality, we obtained primary endometrial epithelial cells and generated ARID1A-KO primary cells using lentiviral CRISPR constructs (**Fig 5A**). Briefly, normal endometrial tissue was processed and put in 2D culture to expand the epithelial cell population. These cells were then transduced with lentivirus containing a CRISPR sgRNA against ARID1A or a non-targeting control (NTC). Cell growth of ARID1A-KO and NTC-transduced cells seeded in 96-well plates challenged with increasing concentrations of AI-1 was measured using an Incyte S3 imaging system. As expected from our cell line data, ARID1A-KO primary cells from three independent donors presented higher sensitivity to AI-1 compared to their NTC counterparts (**Fig 5B** and **Fig S5A**). Validation of ARID1A status by western blot confirmed the knockout of ARID1A in these samples (**Fig 5C**). In further support to our findings, ARID1A-KO cells also presented higher levels of the DNA damage marker γH2AX, which was exacerbated by the addition of AI-1 (**Fig 5C**). In parallel, we also grew primary cells from one patient into a 3D organoid culture and assessed the survival of ARID1A-WT (NTC control) and ARID1A-KO organoids (sgARID1A) subjected to increasing concentrations of AI-1. Transduced cells were tracked using the tdTomato reporter contained in the lentiviral vector, and IHC staining was used to validate the ARID1A-status of the samples (**S5B)**. We found that AI-1 treatment resulted in dose-dependent selective killing of ARID1A-KO organoids compared to their NTC counterparts (**Fig S5C**). Morphological assessment of these organoids further confirmed a general decrease in size and a darkening in color typically associated with necrosis. Overall, these results confirm that the KEAP1-ARID1A synthetic lethal relationship is conserved in primary epithelial cells derived from endometrial tissue samples and supports the translational potential of our findings.

DISCUSSION

Despite a high incidence of mutations across cancers, precision medicine options for patients harboring ARID1A mutations in cancer remains limited and unspecific. To identify genetic dependencies of ARID1A-deficient CCOC cells to advise on alternative treatments, we performed two genome-wide CRISPR screens in an isogenic cell line model of ARID1A loss in RMG-1 cells. Our screen identified known ARID1A synthetic lethal partners in SMARCC1 and DDX19A[41]. Known ARID1A synthetic lethal paralogue ARID1B was only identified as significant in one of the two biological replicates, highlighting the noise of this approach and the need for replicates. The overlap between our two screens identified a consensus dataset of 103 genes that are important for survival when ARID1A is lost (**Fig 1C**). While this overlap was statistically significant, our data also highlights the variability between biological replicates of CRISPR screening experiments.

It is worth noting that the top hit from our screen, pyridoxamine 5'-phosphate oxidase (PNPO), is a metabolic enzyme involved in the breakdown of vitamin B6. Despite no reports of ARID1A loss impacting vitamin B6 metabolism, there are many reports highlighting the

metabolic consequences of ARID1A mutations[23,25,52]. It is therefore possible that loss of ARID1A, through metabolic reprogramming, would induce sensitivity to PNPO depletion. Further research will be needed to confirm this hypothesis and whether vitamin B6 biology relates in any way to ARID1A-deficient tumor fitness. The 2nd hit from our screen was assigned to the CTD Small Phosphatase 1 (CTDSP1), which functions in the regulation of transcriptional elongation by RNAPII. While we did not test effects of CTDSP1 depletion beyond the screen, there is strong evidence that loss of ARID1A results in defects in transcriptional elongation[21]. In fact, ARID1A deficiency impairs promoter proximal pausing dynamics, a crucial step for productive transcriptional elongation[21]. We hypothesize that inhibition of CTDSP1 would exacerbate this phenotype and perhaps sensitize ARID1A-KO cells to CTDSP1 depletion. Ultimately, our CRISPR screen identified strong potential synthetic lethal dependencies of ARID1A-KO cells. Given that ARID1A physically interacts with NRF2, and that the disruption of this interaction results in fitness defects[24], we chose to focus on KEAP1.

To validate the findings from our CRISPR screen, we assessed the sensitivity of KEAP1 depletion by siRNA or a small molecules inhibitor (i.e., AI-1) in two isogenic cell line models of ARID1A loss. While there are notable differences between our RMG-1 and RPE1 cell line models, ARID1A-loss sensitized cells to KEAP1 depletion by siRNA in both cellular backgrounds. Similarly, we observed sensitivity to KEAP1 inhibition by AI-1 in both cell lines when ARID1A is lost, as well as a strong correlation in a panel of CCOC cell lines. AI-1 covalently modifies the Cys151 residue of KEAP1, disrupting the ability of KEAP1 to serve as an adaptor for CUL3-KEAP1 ubiquitin ligase complex, causing stabilization and transcriptional activation of NRF2[45]. We also tested sensitivity to SFN, an NRF2 inducer targeting KEAP1's C-terminal cysteine residues akin to AI-1[53,54], and observed a significant growth impairment in our RPE1 isogenic cell line model of ARID1A-loss but not the RMG-1 derived model (**Fig S2D**). We suggest that the differences in phenotypes observed with SFN can partially be explained by cell-type specific metabolic differences. In addition, we further validated the sensitivity of ARID1A-KO cells to AI-1 in patient-derived endometrial progenitor cells and organoids (**Fig 5** and **Fig S5**). Our findings confirmed the observations we made in cell lines, suggesting that the synthetic lethal relationship between KEAP1 and ARID1A could be applicable to the clinic.

To gain further insight on the potential mechanism underlying the synthetic lethality between KEAP1 and ARID1A, we sought to determine if NRF2 signalling may be disrupted following ARID1A-loss. Building on work by Wu *et al.*[22], we performed a differential gene expression analysis that identified large subsets of genes that are disrupted when ARID1A is lost. Among these, polycomb repressive complex 2 (PRC2) target genes were highly enriched within the DGE dataset, as seen by the enrichment of the PRC2 subunits SUZ12 and EZH2 (**Fig 3B)**. This is unsurprising considering that PRC2 and the BAF complex have antagonistic roles in the regulation of gene expression [26,55]. Accordingly, EZH2 inhibition in ARID1A-deficient cells has been reported to behave in a synthetic lethal manner [56,57]. Interestingly, our DGE analysis also revealed that NRF2 (NFE2L2) target genes are highly enriched among both the up-regulated, and to a lesser extent, down-regulated genes (**Fig 3B**). Furthermore, we analyzed pan-cancer TCGA data that revealed a significant upregulation of KEAP1 mRNA levels in ARID1A-mutated tumours for multiple subtypes, including stomach adenocarcinoma (STAD)

and colon adenocarcinoma (COADREAD) (**Fig 3D** and **Fig S3A**). Unfortunately, limitations in data availability prevented us from assessing this trend in ovarian carcinoma subtypes specifically. These results suggest that some tissues up-regulate KEAP1 when ARID1A is mutated, suggesting that KEAP1 may serve as a biomarker to inform on treatment modalities for ARID1A-deficient cancers beyond the ovary.

While our findings supported the notion that KEAP1-NRF2 signalling is disrupted in ARID1A-KO cells, we found that knocking down NRF2 by siRNA did not rescue the sensitivity of ARID1A-KO cells to AI-1 (**Fig 3G**). In addition, we observed that dual depletion of KEAP1 and NRF2 by siRNA resulted in an epistatic phenotype, with comparable fitness defects to siKEAP1. Although we cannot rule out that aberrant NRF2 signalling may be partially responsible for the selective killing of ARID1A-KO cells following KEAP1 perturbation, our findings suggest that functions of KEAP1 outside of NRF2 regulation may underlie the genetic dependency we report herein. While KEAP1 has been extensively studied in the context of NRF2 regulation, it also has reported roles in the regulation of proteostasis, cytoskeleton formation and the cell cycle[58,59]. In fact, KEAP1 is an essential component of the KEAP1-CUL3-RBX1 ubiquitin ligase complex that targets various proteins for degradation, and also functions in autophagy with its interacting partner, p62[58,60,61]. Since defects in proteostasis result in pleiotropic effects in the cell, it is possible that such changes could sensitize ARID1A-KO cells to KEAP1 perturbation. Additionally, KEAP1 has been shown to interact with proteins like BRCA1 and PALB2, which may influence DNA repair pathway choice and cell cycle regulation. Based on our genome instability data, we suspect that changes in DNA repair pathway choice may contribute to the genome instability phenotypes we observed in ARID1A-KO cells depleted for KEAP1, though more research will be necessary to confirm this hypothesis. Furthermore, two groups have identified MCM3, a component of the replicative DNA helicase complex, as a substrate of KEAP1[62,63]. While the exact function of this interaction remains unknown, Mulvaney *et al*. showed that KEAP1 associates with chromatin during S-phase. The authors suggest that KEAP1 plays a role in monitoring replication fork progression and the coordination of replisome activity. Overall, these results point towards an NRF2-independent role for KEAP1 in the maintenance of genome integrity, which may be further exacerbated when ARID1A is lost.

One potential limitation of our study was the relatively high concentrations of AI-1 needed to elicit strong KEAP1 inhibition (as measured by NRF2 induction). While off-target reactivity of AI-1 and sulforaphane, particularly affecting HDAC1 levels, has been documented[45,64], we did not observe major changes in HDAC1 levels following treatment with either of these inhibitors (**Fig S3F**). However, we found that KEAP1 inhibition by sub-lethal doses of AI-1 (i.e., 50μM) exacerbated the genome instability phenotypes that are observed in ARID1A-KO cells, namely increasing DNA replication stress, DNA damage and micronuclei formation. Building on these findings, we also found that sublethal concentrations of AI-1 in combination with ceralasertib allowed to selectively kill ARID1A-KO cells. This data suggests that combination therapy potentiates the effects of AI-1 and may allow for lower concentrations of the drug to selectively eliminate ARID1A-KO cells. Importantly, we also further validated some of our findings using siRNA knockdown of KEAP1 as a complementary approach. Although knockdown of KEAP1 may also potentially result in a different spectrum of

off-target effects, our results converge to suggest that KEAP1 functions in the maintenance of genome integrity in ARID1A-deficient cancer cells. Ultimately both understanding the mechanism of action and generating more potent KEAP1 inhibitors will be key to impacting ARID1A-deficient tumours clinically.

While our group is the first to our knowledge to document a synthetic lethal interaction between KEAP1 and ARID1A, consequences of ARID1A loss on NRF2 signalling have been reported. Another group has reported that ARID1A-loss causes glutathione metabolism deficiencies, which sensitizes ARID1A-KO cells to SLC7A11 depletion[24]. The authors showed that this synthetic lethal relationship was partially explained by the loss of an interaction between ARID1A and NRF2, which in turn regulates SLC7A11 expression. While the role of KEAP1 on this genetic dependency has not been explored, additional evidence suggests that KEAP1-mediated signalling is important in ARID1A-deficient cells. In fact, bromodomain and extra-terminal domain inhibitors (BETi) have been used to selectively kill ARID1A-KO cells; particularly the inhibitor JQ-1, which targets BRD4. While the authors suggest that this toxicity is due to transcriptional changes associated with an increased BRD4 recruitment to chromatin, BRD4 inhibition by JQ-1 has been shown to affect KEAP1-NRF2 signalling, supporting the idea that KEAP1 is perhaps a regulator of fitness in ARID1A-deficient cells[65–67]. Additionally, loss of other BAF complex subunits has been associated with the dysregulation of KEAP1-NRF2 signalling. For instance, mutations in the catalytic subunit BRG1 have been associated with changes in NRF2-mediated gene expression[68]. Overall, this suggests that there exists a convergence in functions between the BAF complex and KEAP1-NRF2 signalling, though further research is needed to explore the nature of this connection. Ultimately, our findings provide a new therapeutic strategy to selectively kill ARID1A-deficient cells. More research will be necessary to understand the mechanistic implications of the KEAP1-ARID1A dependency to inform on novel treatments against ARID1A-KO tumours.

METHODS

Cell culture conditions

CCOC cell lines (RMG-1, RMG-II, JHOC-5, JHOC-7, OVCA 429, OVISE and OVMANA) were cultured in RPMI 1640 supplemented with 10% FBS and 1% penicillin/streptomycin at 37°C, supplied with 5% CO_2. RPE1-hTERT Flag-Cas9 p53-WT cells were cultured in DMEM/Ham's F12 50:50 mix 1X (with L-glut and 15mM HEPES) supplemented with 10% FBS and 1% penicillin/streptomycin at 37°C, supplied with 5% CO_2.

RPE1 ARID1A-KO cell line generation:

RMG-1 ARID1A-WT and ARID1A-KO cells were a generous gift from the Huntsman Lab[1]. The CCOC cell line panel (JHOC-5/7, OVISE, OVMANA, OVCA 429 and RMG-II) were also obtained from the Huntsman Lab.

RPE1-hTERT Flag-Cas9 p53-WT cells[69] were a generous gift from the Durocher Lab. ARID1A was knocked out with CRISPR using the Alt-R CRISPR-Cas9 System from Integrated DNA Technologies (IDT). Custom crRNA were designed using the Custom Alt-R CRISPR-Cas9 guide

RNA tool (sequence: TACGGCTTCGGGCAACCCTA, position: 26696844+, IDT ID: Hs.Cas9.ARID1A.1.AA) targeting exon1 of ARID1A. RPE-1-hTERT p53-WT cells stably expressing Cas9 endonuclease were reverse transfected (RNAiMAX reagent, Thermo Fisher Scientific) with the Alt-R CRISPR-Cas9-crRNA complexed with Alt-R CRISPR-Cas9-tracrRNA–ATTO550 (final concentration of 10nM). FACS cell sorting isolated ATTO 550-positive cells and were expanded and sorted again into single cell populations in a 96-well plate. Following outgrowth, genomic DNA was purified, and knockout scores were determined for individual clones from Sanger sequencing data using the Synthego ICE Analysis tool[70] (v3). Additional validation of knockouts was performed by western blot (**Fig S1D-E**).

Generation of NRF2^{E79Q} dox-inducible cell lines

The pIND20-NRF2^{E79Q}-HA plasmid was a generous gift from Bernard Weissman. The plasmid was transformed into bacteria for amplification and validated by sequencing (**Table S4, Sheet 2**). To produce lentiviral particles for stable expression of the construct, 8x10^6 HEK-293T cells were transfected in a 15-cm culture dish. Cells were transfected using the TransIT-LT1 Transfection reagent (Mirus, MIR 2305, 3µL/µg of DNA) with 4.8µg psPAX2, 3.8µg pMD2.G and 8µg pIND20-NRF2^{E79Q}-HA DNA 24-hours after cells were seeded. After 24 hours of transfection, the media was replaced with high-BSA growth media (DMEM + 1.1g/100mL BSA + 1X Pen/Strep) for viral harvest. Lentiviral particles were harvested 48-hours post-transfection, and viral particles were concentrated by ultracentrifugation (25,000g, 4°C, 1.5 hours), resuspended in OPTI-MEM and frozen at -80°C for future use. To generate the stable cell lines, 1x10^6 RMG-1 cells were infected at a MOI between 0.2-0.4 in the presence of 8µg/mL polybrene. The infected cells were selected for 96 hours in media containing 800 µg/mL geneticin (Thermo CAT: 10131027).

TKOv3 library cloning and viral preparation

The Toronto human knockout pooled library (TKOv3) was a gift from Jason Moffat (Addgene #90294). The library was amplified in bacteria as described in the Moffat protocol on Addgene (https://www.addgene.org/pooled-library/moffat-crispr-knockout-tkov3/). The amplified sgRNA library was packaged into lentiviral particles using HEK293T/17 cells by co-transfection with psPAX2 and pMD2.G viral plasmids (1:1:1 molar ratio). To produce viral particles at scale, 510x10^6 cells were transfected in 60 15-cm culture dishes. Each dish was transfected using the TransIT-LT1 Transfection reagent (Mirus, MIR 2305, 3µL/µg of DNA) with 4.8µg psPAX2, 3.8µg pMD2.G and 8µg library DNA 24-hours after cells were seeded. After 24 hours of transfection, the media was replaced with high-BSA growth media (DMEM + 1.1g/100mL BSA + 1X Pen/Strep) for viral harvest. Lentiviral particles were harvested twice at 48-hours and 72-hours post-transfection. Both harvests were pooled, viral particles were concentrated by ultracentrifugation (25,000g, 4°C, 1.5 hours) and frozen at -80°C for future use.

TKOv3 library viral transduction and titration

Viral titre was assessed to determine the multiplicity of infection (MOI) of the concentrated viral particles. RMG-1 ARID1A-WT and ARID1A-KO cells were seeded at a density of 2.5x10^6 cells/well in 12-well plates and spin-fected (2000 rpm for 2 hours at 37°C) with

increasing concentrations of virus in the presence of 8µg/mL polybrene (Millipore TR-003-G lot#3287963). The next day, the cells were split into 6-well plates at a density of 0.5x106 cells/well and subjected to 2µg/mL puromycin (Sigma P8833) for selection of infected cells. Cells not transduced with the library (no virus control) did not survive past 24 hours of puromycin selection (2µg/mL). After 48-hours of selection, all cells in all wells were counted to determine the viral volume that resulted in 20-40% survival in puromycin (corresponding to an MOI of 0.2-0.4 assuming an independent infection rate).

CRISPR knockout pool generation

The dropout CRISPR screen was performed in biological duplicates, in an adapted version of the Mair *et al.* protocol[71]. ARID1A-WT and ARID1A-KO RMG-1 cells were transduced with sgRNA libraries at a multiplicity of infection of (MOI) between 0.2 and 0.4, aiming for coverage of, on average, >500 cells per sgRNA reagent. For genome-wide screens, 120 million cells were transduced by "spin-fection" (2 hours, 2000rpm, 37°C) per cell line in 12-well plates ($2.5x10^6$ cells per well) using the appropriate volume of viral particles for MOI of 0.2-0.4 and 8µg/mL polybrene. Two additional wells per cell line were also plated to account for no puromycin and no virus controls to assess MOI at time 0 (T0). Media was aspirated and refreshed following the infection and cells were incubated overnight. The following, the cells were split, pooled, and seeded at $8x10^6$/plate in 150mm dishes in media containing 2µg/mL puromycin. Additional plates were seeded to assess MOI (no-puromycin, no-virus and virus-infected). Forty-eight hours post-selection with puromycin, the cells were split, and MOI was assessed. Time 0 samples were frozen to assess initial library representation ($20x10^6$ cells - >250X), and the remainder of cells were maintained in culture and split as needed to ensure confluence did not exceed 90%. Cells were harvested and frozen as "dry" pellets (-80°C) at relevant time points for subsequent sgRNA enrichment assessment (described below).

Genomic DNA extraction and precipitation

Genomic DNA extraction and precipitation was performed according to the method described in the TKOv3 protocol described by Mair *et al.*[71] using the QIAamp Blood Maxi kit (cat no. 51194) and RNase A (cat no. 19101).

Library preparation and sequencing

The sgRNA libraries were prepared using two-steps of PCR as described by Mair *et al.*[71]: 1) amplify the sgRNA region within genomic DNA; 2) amplify sgRNAs with Illumina TruSeq adapters with i5 and i7 indices (see **Table S4**). These indices are unique sequences that are added to DNA samples during library preparation and act as sample identifiers during multiplex sequencing. All PCR steps were performed using the NEBNext Ultra II Q5 Master Mix high-fidelity polymerase. For PCR #1, the thermocycling parameters were 98°C for 30s, 25 cycles of (98°C for 10s, 66°C for 30s, 72°C for 15s), and 72°C for 2 minutes. In each PCR #1 reaction, we used 3.5µg of gDNA. For each sample, the necessary number of PCR #1 reactions was used to capture the appropriate representation of the screen. For instance, assuming a diploid genome is ~7.2 pg and one guide-RNA per genome, 100 µg of genomic DNA yields ~200- fold coverage of the TKOv3 library. In this example, at least 29 PCR#1 reactions were necessary to capture 200X representation of the library for each replicate.

PCR #1 products were pooled for each biological samples and 5 µL was used for amplification and unique barcoding in PCR #2. The thermocycling parameters for PCR#2 were 98°C for 30s, followed by 10 cycles of (98°C for 10s, 55°C for 30s and 65°C for 15s), and 65°C for 5 minutes. The PCR #2 products were validated using gel electrophoresis and purified using the QIAquick Gel extraction kit (QIAGEN). The purified libraries were then quantified by Nanodrop and Qubit prior to sequencing on an Illumina MiSeq (2 samples per lane for >100X coverage).

Amplicon scoring, guide-RNA enrichment and hit identification

Deep amplicon sequencing data was processed for sgRNA representation using custom scripts. To summarize, the sequencing reads were first de-multiplexed using the 8-bp barcodes in the forward primer, then using the 8-bp barcodes in the reverse primers. De-multiplexed reads were trimmed to leave only the 20-bp spacer (sgRNA) sequences. The sgRNA sequences were then mapped to the reference TKOv3 library sgRNA sequences using Bowtie 2[35]. For mapping, no mismatches were allowed, and mapped sgRNA sequences were quantified by counting the total number of reads.

Fitness scores were assigned to each gene by integrating the read counts from individual sgRNAs using BAGEL2 (each replicate analysed independently)[72]. Genes with a positive Bayes Factor and an FDR cut-off of 0.05 were determined important for fitness across datasets, and hits that were unique to the ARID1A-KO datasets (i.e. not overlapping between ARID1A-WT and KO) were identified as synthetic lethal to ARID1A. The consensus dataset of synthetic lethal partners of ARID1A corresponds to the intersection of ARID1A-KO specific hits from both biological replicates of the screen.

Gene ontology (GO) analysis

Gene ontology analysis for biological processes was performed using DAVID v6.8[73]. Gene ontology analysis for target genes of transcription factors was performed using the ENCODE and ChEA datasets from EnrichR[74].

Incucyte growth assay

Cells were seeded at 5,000 (RPE1) or 10,000 (RMG-1) cells per well in a clear bottom 96-well plate on day 0. For drug treatments, cells were treated with indicated drug concentrations on day 1 and placed in an IncuCyte S3 live-cell imaging system contained in an incubator kept at 37 °C and 5% CO2. Images were taken at 2-hour intervals in quadruplicate/well for 72-96 hours.

For experiments with siRNA, $2x10^5$ cells per well were reverse transfected onto 25nM siRNA complex in a 6-well plate. Cells were incubated overnight, and media was replaced the following day. 48-hours post transfection, the cells were split and counted. Cells were seeded at 10,000 cells per well in a 96-well plate, while the remainder of cells was lysed for analysis by western blot. The 96-well plate was treated with drugs as indicated in figure legends, and placed in an IncuCyte S3 live-cell imaging system contained in an incubator kept at 37 °C and 5% CO2. Images were taken at 2-hour intervals in quadruplicate for 72-96 hours.

RNA interference

2×10^5 cells were reverse-transfected in 6-well plates with Flexitube siRNA constructs (Qiagen) targeting KEAP1 (KEAP1_5 or KEAP1_8), NRF2 (NRF2_10), or a non-targeting control

(siCTRL) at concentrations of 25 nM with HiPerFect Transfection Reagent (Qiagen, #301705) according to the manufacturer's protocol. Target sequences are available in **Table S4**. Cells were cultured for 48 h after transfection and before subsequent analysis.

Alternatively, for reverse transfection, cells were seeded at 5,000 (RPE1) or 10,000 (RMG-1) cells per well in 24-well plates on day 0. On day 1, cells were transfected with 25nM siRNA (final concentration).

Crystal violet proliferation/viability assay

KEAP1 siRNA survival: For siRNA experiments, cells were seeded at 5,000 (RPE1) or 10,000 (RMG-1) cells per well in 24-well plates on day 0. On day 1, cells were transfected with 25nM siRNA (final concentration). Cells were fixed for crystal violet staining after 7 days of outgrowth on Day 8.

For experiments with drug treatments, cells were seeded at 5,000 (RPE1, OVCA 429) or 10,000 (RMG-1, RMG-II, OVMANA, OVISE, JHOC-5/7) cells per well in 24-well plates, and incubated overnight prior to addition of the drug. Cells were fixed for crystal violet staining after outgrowth of 7 days on day 8.

For experiments with RMG-1 p.IND20-NRF2-E79-HA expressing cells, 10,000 cells were seeded in a 6-well plate on Day 0. On day 1, doxycycline was added to the media at concentrations indicated in figure legends. Media was changed on day 4 to replenish doxycycline. Cells were fixed for crystal violet staining on day 7.

Briefly, cells were washed with PBS and fixed with 3.7% formaldehyde for 15 minutes at RT. Cells were washed with PBS and stained with crystal violet for 30 minutes at RT, after which cells were washed with distilled H_2O until no residual crystal violet could be observed. The plates were dried at RT overnight. The following day, the plates were incubated for 15 minutes at RT (in dark) following the addition of 500µL of 10% acetic acid in methanol. The absorbance at 570nm was measured using a Tecan Infinite M200Pro plate reader.

Immunofluorescence

For all immunofluorescence experiments, cells were grown on coverslips overnight. For experiments with drug treatments, cells were treated at indicated concentrations for 24 hours prior to fixation. For siRNA transfections, cells were reverse transfected at time of seeding with appropriate siRNA concentrations and grown for 48 hours prior to fixation.

Cells were fixed with 4% paraformaldehyde for 10 minutes and permeabilized with 0.2% Triton X-100 for 10 minutes on ice. After permeabilization, cells were washed with PBS and blocked in 3%BSA, 0.1% Tween 20 in 4X saline sodium citrate buffer (SSC) for 1 hour at room temperature. Cells were then incubated with primary antibodies (**Table S4**) overnight at 4°C. Following PBS wash, cells were then incubated with Alexa-Fluor-488 or 568-conjugated secondary antibodies for 1 hour at room temperature, washed with PBS for 10 minutes 3 times, and stained with DAPI before mounting and imagining on LeicaDMI8 microscope at 100X magnification. ImageJ was used for image processing and quantification[75]. For assessment of micronuclei formation, DAPI staining was used to identify micronuclei-positive cells, which were quantified as a percentage of all cells analyzed.

Western Blotting

Whole-cell lysates were prepared with RIPA buffer containing protease inhibitor (Sigma) and phosphatase inhibitor (Roche Applied Science) cocktail tablets and the protein concentration were determined by Bio-Rad Protein assay (Bio-Rad). Equivalent amounts of protein were resolved by SDS-PAGE and transferred to polyvinylidene fluoride microporous membrane (Millipore), blocked with 1.5% BSA in H20 containing 0.1% Tween-20 (TBS-T), and membranes were probed with the primary antibodies listed in (**Table S4**). Secondary antibodies were conjugated to horseradish peroxidase (HRP) and peroxidase activity was visualized using Chemiluminescent HRP substrate (Thermo Scientific). For quantification of protein samples, western blot images were analyzed using Image Lab Software for PC (v6.1). KEAP1 protein levels (Adj. Volume Int.) were normalized to GAPDH loading control and compared between samples.

TCGA dataset analysis

mRNA expression levels were obtained from the TCGA cBioportal (RSEM - Batch normalized from Illumina HiSeq_RNASeqV2). Correlations of ARID1A and KEAP1 were analyzed using all samples (n = 10,071). For stratification by ARID1A-mutational status, ARID1A-mutated samples were sub-setted using VEG scores of “High” (meaning high impact on protein function - e.g., frameshift or loss). Cancer subtypes with at least 5 data points for either of ARID1A-WT or ARID1A-KO were selected for analysis.

Differential gene expression analysis

RNA-seq data for RMG-1 cells isogenic for ARID1a was obtained from Wu *et. al*[22]. Differentially expressed genes were generated using DESEQ2[47].

Culture of patient-derived endometrial progenitor cells and organoids

Primary endometrial epithelial cells and organoids were derived as previously reported by Cochrane *et al.*[78] from hysterectomy tissue from surgeries for non-cancer reasons performed at the Vancouver General Hospital (VGH) and University of British Columbia (UBC) hospitals. Tissues were collected as part of the OVCARE’s Gynaecologic Tissue Bank. These studies were approved by the Institutional Review Board (IRB) of UBC and British Columbia Cancer Agency (H05-60119), and use of the tissue for research purposes was approved by written informed consent by the patients.

Primary endometrial epithelial cell culture in 2D: Cells were seeded in 6 well plates to be transfected by ARID1A and non-targeting control CRISPR lentiviruses. ARID1A (12354, cell signaling, 1/1000) western blot was performed to confirm the downregulation of ARID1A protein in sgARID1A infected cells compare to NTC controls. Then, cells were seeded at a density of 1000 cells/well in 96 well plates. KEAP1 inhibitor treatment was performed after 24h using increasing concentrations and the plates were placed into an IncuCyte S3 imaging system to assess proliferation for 7 days.

Primary endometrial epithelial cell culture in 3D (organoids): After 72h in organoid culture, the cells were subjected to KEAP1 inhibitor treatment at indicated concentrations. Organoid growth was monitored for 10 days post treatment in culture.

Immunohistochemistry

For immunohistochemical analyses, non-treated organoids were formalin-fixed and paraffin-embedded. The Matrigel was dissolved in cold PBS, and the organoids were fixed in 4% formaldehyde for 1 h at room temperature. After centrifugation, the formaldehyde was removed, and the organoids were resuspended in 70% ethanol. The fixed organoids were then suspended in Histogel (Thermo Fisher). After dehydration in a series of alcohols, the organoids were embedded in paraffin. 4µm sections of organoid blocks were stained with ARID1A antibody (ab182560, 1/3000) on the automated Leica BOND RX system (Leica Biosystems).

Statistical analysis and reproducibility

Statistical analysis was performed using GraphPad Prism 9. Experiments were repeated three times unless otherwise stated. The representative images were shown unless otherwise stated. Quantitative data were expressed as means ± SEM unless otherwise stated. Analysis of variance (ANOVA) was used to identify significant differences in multiple comparisons.

ACKNOWLEDGEMENTS

We thank DGH and Michael Anglesio for the RMG-1 ARID1A-WT and ARID1A-KO cells, as well as the other CCOC cell lines. The RPE1-hTERT Flag-Cas9 p53-WT cells[62] were a generous gift from the Durocher Lab. We also thank Rodrigo Vallejos and Dawn Cochrane for their support with data analysis and organoid culture respectively. We also acknowledge Grace Cheng, Fraser Johnson, Dylan Farnsworth and the Morin Lab for their assistance with the IncuCyte. The pIND20-NRF2^{E79Q}-HA construct was a generous gift from Bernard Weissman. Some of the results shown herein are in whole or part based upon data generated by the TCGA Research Network: https://www.cancer.gov/tcga. We also thank Arun Kumar for the insightful discussions that helped shape this manuscript. LAF would also like to acknowledge René Fournier, for providing continuous support through this work.

FUNDING

LAF holds a CIHR Frederick Banting and Charles Best doctoral scholarship and a UBC Four Year Fellowship. This work was supported by a Terry Fox Research Institute Program Project grant to PCS, MH and DGH.

DECLARATION OF INTERESTS

LAF is a member of the Office of the Canada Chief Science Advisor Youth Council (CSA-YC). PCS is CEO of Arrowsmith Genetics Inc.

LITERATURE CITED

1. Wiegand, K. C. *et al.* ARID1A mutations in endometriosis-associated ovarian carcinomas. *N. Engl. J. Med.* **363**, 1532–1543 (2010).
2. Jones, S. *et al.* Frequent mutations of chromatin remodeling gene ARID1A in ovarian clear cell carcinoma. *Science* **330**, 228–231 (2010).
3. Ashizawa, M. *et al.* Prognostic role of ARID1A negative expression in gastric cancer. *Sci. Rep.* **9**, 6769 (2019).
4. Wang, D. *et al.* Decreased Expression of the ARID1A Gene Is Associated with Poor Prognosis in Primary Gastric Cancer. *PLOS ONE* **7**, e40364 (2012).
5. Zhu, Y. P. *et al.* Loss of ARID1A expression is associated with poor prognosis in patients with gastric cancer. *Hum. Pathol.* **78**, 28–35 (2018).
6. Wang, T. *et al.* Downregulation of ARID1A is correlated with poor prognosis in non-small cell lung cancer. *Transl. Cancer Res.* **9**, 4896–4905 (2020).
7. Yang, H., Huo, J. & Li, X. Identification and validation of a five-gene prognostic signature for hepatocellular carcinoma. *World J. Surg. Oncol.* **19**, 90 (2021).
8. Yim, S. Y. *et al.* Low ARID1A Expression is Associated with Poor Prognosis in Hepatocellular Carcinoma. *Cells* **9**, 2002 (2020).
9. He, F. *et al.* Decreased expression of ARID1A associates with poor prognosis and promotes metastases of hepatocellular carcinoma. *J. Exp. Clin. Cancer Res.* **34**, 47 (2015).
10. Cho, H. D. *et al.* Loss of Tumor Suppressor ARID1A Protein Expression Correlates with Poor Prognosis in Patients with Primary Breast Cancer. *J. Breast Cancer* **18**, 339–346 (2015).
11. Ayhan, A. *et al.* Loss of ARID1A expression is an early molecular event in tumor progression from ovarian endometriotic cyst to clear cell and endometrioid carcinoma. *Int J Gynecol Cancer* **22**, 1310–5 (2012).
12. Lowery, W. J. *et al.* Loss of ARID1A-associated Protein Expression Is a Frequent Event in Clear Cell and Endometrioid Ovarian Cancers. *Int. J. Gynecol. Cancer* **22**, 9–14 (2012).
13. Maeda, D. *et al.* Clinicopathological Significance of Loss of ARID1A Immunoreactivity in Ovarian Clear Cell Carcinoma. *Int. J. Mol. Sci.* **11**, 5120–5128 (2010).
14. Yamamoto, S., Tsuda, H., Takano, M., Tamai, S. & Matsubara, O. PIK3CA mutations and loss of ARID1A protein expression are early events in the development of cystic ovarian clear cell adenocarcinoma. *Virchows Arch. Int. J. Pathol.* **460**, 77–87 (2012).
15. Choi, J. Y. *et al.* Ovarian Clear Cell Carcinoma Sub-Typing by ARID1A Expression. *Yonsei Med. J.* **58**, 59–66 (2017).
16. Katagiri, A. *et al.* Frequent loss of tumor suppressor ARID1A protein expression in adenocarcinomas/adenosquamous carcinomas of the uterine cervix. *Int. J. Gynecol. Cancer Off. J. Int. Gynecol. Cancer Soc.* **22**, 208–212 (2012).
17. Heinze, K. *et al.* Validated biomarker assays confirm that ARID1A loss is confounded with MMR deficiency, CD8+ TIL infiltration, and provides no independent prognostic value in endometriosis-associated ovarian carcinomas. *J. Pathol.* **256**, 388–401 (2022).
18. Mandal, J., Mandal, P., Wang, T.-L. & Shih, I.-M. Treating ARID1A mutated cancers by harnessing synthetic lethality and DNA damage response. *J. Biomed. Sci.* **29**, 71 (2022).
19. Tsai, S. *et al.* ARID1A regulates R-loop associated DNA replication stress. *PLoS Genet.* **17**,

e1009238 (2021).
20. Zhao, B. *et al.* ARID1A promotes genomic stability through protecting telomere cohesion. *Nat. Commun.* **10**, 4067 (2019).
21. Trizzino, M. *et al.* The Tumor Suppressor ARID1A Controls Global Transcription via Pausing of RNA Polymerase II. *Cell Rep.* **23**, 3933–3945 (2018).
22. Wu, S. *et al.* ARID1A spatially partitions interphase chromosomes. *Sci Adv* **5**, eaaw5294 (2019).
23. Goldman, A. R. *et al.* The Primary Effect on the Proteome of ARID1A-mutated Ovarian Clear Cell Carcinoma is Downregulation of the Mevalonate Pathway at the Post-transcriptional Level. *Mol Cell Proteomics* **15**, 3348–3360 (2016).
24. Ogiwara, H. *et al.* Targeting the Vulnerability of Glutathione Metabolism in ARID1A-Deficient Cancers. *Cancer Cell* **35**, 177-190 e8 (2019).
25. Zhang, X., Shetty, M., Clemente, V., Linder, S. & Bazzaro, M. Targeting Mitochondrial Metabolism in Clear Cell Carcinoma of the Ovaries. *Int. J. Mol. Sci.* **22**, 4750 (2021).
26. Zhang, W. *et al.* The BAF and PRC2 Complex Subunits Dpf2 and Eed Antagonistically Converge on Tbx3 to Control ESC Differentiation. *Cell Stem Cell* **24**, 138-152.e8 (2019).
27. Kadoch, C., Copeland, R. A. & Keilhack, H. PRC2 and SWI/SNF Chromatin Remodeling Complexes in Health and Disease. *Biochemistry* **55**, 1600–14 (2016).
28. Wilson, M. R. *et al.* SWI/SNF Antagonism of PRC2 Mediates Estrogen-Induced Progesterone Receptor Expression. *Cells* **11**, 1000 (2022).
29. Bitler, B. G. *et al.* Synthetic lethality by targeting EZH2 methyltransferase activity in ARID1A-mutated cancers. *Nat. Med.* **21**, 231–238 (2015).
30. Yamada, L. *et al.* Selective sensitivity of EZH2 inhibitors based on synthetic lethality in ARID1A-deficient gastric cancer. *Gastric Cancer Off. J. Int. Gastric Cancer Assoc. Jpn. Gastric Cancer Assoc.* **24**, 60–71 (2021).
31. Sen, M. *et al.* ARID1A facilitates KRAS signaling-regulated enhancer activity in an AP1-dependent manner in colorectal cancer cells. *Clin. Epigenetics* **11**, 92 (2019).
32. Berns, K. *et al.* ARID1A mutation sensitizes most ovarian clear cell carcinomas to BET inhibitors. *Oncogene* **37**, 4611–4625 (2018).
33. Wu, C. *et al.* Targeting AURKA-CDC25C axis to induce synthetic lethality in ARID1A-deficient colorectal cancer cells. *Nat. Commun.* **9**, 3212 (2018).
34. Hart, T. *et al.* Evaluation and Design of Genome-wide CRISPR/Cas9 Knockout Screens. *bioRxiv* (2017) doi:10.1101/117341.
35. Langmead, B. & Salzberg, S. L. Fast gapped-read alignment with Bowtie 2. *Nat. Methods* **9**, 357–359 (2012).
36. Improved analysis of CRISPR fitness screens and reduced off-target effects with the BAGEL2 gene essentiality classifier | Genome Medicine | Full Text. https://genomemedicine.biomedcentral.com/articles/10.1186/s13073-020-00809-3.
37. Mittal, P. & Roberts, C. W. M. The SWI/SNF complex in cancer — biology, biomarkers and therapy. *Nat. Rev. Clin. Oncol.* **17**, 435–448 (2020).
38. Mathur, R. ARID1A loss in cancer: Towards a mechanistic understanding. *Pharmacol Ther* **190**, 15–23 (2018).
39. Hodges, C., Kirkland, J. G. & Crabtree, G. R. The Many Roles of BAF (mSWI/SNF) and PBAF Complexes in Cancer. *Cold Spring Harb Perspect Med* **6**, (2016).

40. Lebedev, T. *et al.* Targeting ARID1A-Deficient Cancers: An Immune-Metabolic Perspective. *Cells* **12**, 952 (2023).
41. Feng, X. *et al.* Genome-wide CRISPR screens using isogenic cells reveal vulnerabilities conferred by loss of tumor suppressors. *Sci. Adv.* **8**, eabm6638 (2022).
42. Tsherniak, A. *et al.* Defining a Cancer Dependency Map. *Cell* **170**, 564-576.e16 (2017).
43. Helming, K. C. *et al.* ARID1B is a specific vulnerability in ARID1A-mutant cancers. *Nat. Med.* **20**, 251–254 (2014).
44. He, F., Ru, X. & Wen, T. NRF2, a Transcription Factor for Stress Response and Beyond. *Int. J. Mol. Sci.* **21**, 4777 (2020).
45. Hur, W. *et al.* A Small-Molecule Inducer of the Antioxidant Response Element. *Chem. Biol.* **17**, 537–547 (2010).
46. Hu, C., Eggler, A. L., Mesecar, A. D. & van Breemen, R. B. Modification of Keap1 Cysteine Residues by Sulforaphane. *Chem. Res. Toxicol.* **24**, 515–521 (2011).
47. Love, M. I., Huber, W. & Anders, S. Moderated estimation of fold change and dispersion for RNA-seq data with DESeq2. *Genome Biol.* **15**, 550 (2014).
48. Taguchi, K. & Yamamoto, M. The KEAP1-NRF2 System in Cancer. *Front. Oncol.* **7**, 85 (2017).
49. Kerins, M. J. & Ooi, A. A catalogue of somatic NRF2 gain-of-function mutations in cancer. *Sci. Rep.* **8**, 12846 (2018).
50. Krupina, K., Goginashvili, A. & Cleveland, D. W. Causes and consequences of micronuclei. *Curr. Opin. Cell Biol.* **70**, 91–99 (2021).
51. Williamson, C. T. *et al.* ATR inhibitors as a synthetic lethal therapy for tumours deficient in ARID1A. *Nat Commun* **7**, 13837 (2016).
52. Ogiwara, H. *et al.* Targeting the Vulnerability of Glutathione Metabolism in ARID1A-Deficient Cancers. *Cancer Cell* **35**, 177-190.e8 (2019).
53. McMahon, M., Lamont, D. J., Beattie, K. A. & Hayes, J. D. Keap1 perceives stress via three sensors for the endogenous signaling molecules nitric oxide, zinc, and alkenals. *Proc. Natl. Acad. Sci. U. S. A.* **107**, 18838–18843 (2010).
54. Dinkova-Kostova, A. T., Fahey, J. W., Kostov, R. V. & Kensler, T. W. KEAP1 and done? Targeting the NRF2 pathway with sulforaphane. *Trends Food Sci. Technol.* **69**, 257–269 (2017).
55. Kadoch, C. *et al.* Dynamics of BAF-Polycomb complex opposition on heterochromatin in normal and oncogenic states. *Nat Genet* **49**, 213–222 (2017).
56. Alldredge, J. K. & Eskander, R. N. EZH2 inhibition in ARID1A mutated clear cell and endometrioid ovarian and endometrioid endometrial cancers. *Gynecol. Oncol. Res. Pract.* **4**, 17 (2017).
57. Kim, K. H. *et al.* SWI/SNF-mutant cancers depend on catalytic and non-catalytic activity of EZH2. *Nat. Med.* **21**, 1491–1496 (2015).
58. Kopacz, A., Kloska, D., Forman, H. J., Jozkowicz, A. & Grochot-Przeczek, A. Beyond repression of Nrf2: An update on Keap1. *Free Radic. Biol. Med.* **157**, 63–74 (2020).
59. Chen, F. *et al.* Different inhibition of Nrf2 by two Keap1 isoforms α and β to shape malignant behaviour of human hepatocellular carcinoma. 2022.07.15.500244 Preprint at https://doi.org/10.1101/2022.07.15.500244 (2022).
60. Shah, S. Z. A. *et al.* p62-Keap1-NRF2-ARE Pathway: A Contentious Player for Selective

Targeting of Autophagy, Oxidative Stress and Mitochondrial Dysfunction in Prion Diseases. *Front. Mol. Neurosci.* **11**, (2018).

61. Komatsu, M. *et al.* The selective autophagy substrate p62 activates the stress responsive transcription factor Nrf2 through inactivation of Keap1. *Nat. Cell Biol.* **12**, 213–223 (2010).
62. Tamberg, N. *et al.* Keap1-MCM3 interaction is a potential coordinator of molecular machineries of antioxidant response and genomic DNA replication in metazoa. *Sci. Rep.* **8**, 12136 (2018).
63. Mulvaney, K. M. *et al.* Identification and Characterization of MCM3 as a Kelch-like ECH-associated Protein 1 (KEAP1) Substrate *. *J. Biol. Chem.* **291**, 23719–23733 (2016).
64. Kopacz, A. *et al.* Overlooked and valuable facts to know in the NRF2/KEAP1 field. *Free Radic. Biol. Med.* **192**, 37–49 (2022).
65. Lv, Y. *et al.* BRD4 Targets the KEAP1-Nrf2-G6PD Axis and Suppresses Redox Metabolism in Small Cell Lung Cancer. *Antioxidants* **11**, 661 (2022).
66. Hussong, M. *et al.* The bromodomain protein BRD4 regulates the KEAP1/NRF2-dependent oxidative stress response. *Cell Death Dis.* **5**, e1195 (2014).
67. Huang, M. *et al.* Brd4 regulates the expression of essential autophagy genes and Keap1 in AML cells. *Oncotarget* **9**, (2018).
68. Song, S. *et al.* Loss of SWI/SNF chromatin remodeling alters NRF2 signaling in non-small cell lung carcinoma. *Mol. Cancer Res. MCR* **18**, 1777–1788 (2020).
69. Hart, T. *et al.* High-Resolution CRISPR Screens Reveal Fitness Genes and Genotype-Specific Cancer Liabilities. *Cell* **163**, 1515–1526 (2015).
70. Hsiau, T. *et al.* Inference of CRISPR Edits from Sanger Trace Data. 251082 Preprint at https://doi.org/10.1101/251082 (2019).
71. Mair, B. *et al.* Essential Gene Profiles for Human Pluripotent Stem Cells Identify Uncharacterized Genes and Substrate Dependencies. *Cell Rep.* **27**, 599-615.e12 (2019).
72. Kim, E. & Hart, T. Improved analysis of CRISPR fitness screens and reduced off-target effects with the BAGEL2 gene essentiality classifier. *Genome Med.* **13**, 2 (2021).
73. Systematic and integrative analysis of large gene lists using DAVID bioinformatics resources - PubMed. https://pubmed.ncbi.nlm.nih.gov/19131956/.
74. Chen, E. Y. *et al.* Enrichr: interactive and collaborative HTML5 gene list enrichment analysis tool. *BMC Bioinformatics* **14**, 128 (2013).
75. Schneider, C. A., Rasband, W. S. & Eliceiri, K. W. NIH Image to ImageJ: 25 years of image analysis. *Nat. Methods* **9**, 671–675 (2012).
76. ENCODE Project Consortium. An integrated encyclopedia of DNA elements in the human genome. *Nature* **489**, 57–74 (2012).
77. Lachmann, A. *et al.* ChEA: transcription factor regulation inferred from integrating genome-wide ChIP-X experiments. *Bioinforma. Oxf. Engl.* **26**, 2438–2444 (2010).
78. Cochrane, D. R. et al. Single cell transcriptomes of normal endometrial derived organoids uncover novel cell type markers and cryptic differentiation of primary tumours. J Pathol 252, 201–214 (2020).

FIGURE LEGENDS

***Figure 1*. Genome-wide CRISPR screen identifies KEAP1 as a synthetic lethal partner of ARID1A**

A) Schematic of CRISPR screening workflow with the TKOv3 library. **B)** Precision-Recall curve assessing CRISPR screen performance of individual replicates (values obtained from BAGEL2 algorithm, **Supplemental Table 1.5-6**). **C)** Overlap of ARID1A-SL hits from both biological replicates of the CRISPR screen. **D)** Top 10 enriched Biological Processes GO terms identified using David v 6.8 ($p<0.05$, with FDR correction) for the ARID1A-KO fitness genes identified by either of our CRISPR screens (n = 1,484 genes, **Supplemental Table 2.1**). **E)** Ranked ARID1A-KO specific hits (average BF from both biological replicates, **Supplemental Table 1.8**). The top 3 hits are labeled on the graph.

Figure 2. ARID1A-KO cells are sensitive to KEAP1 depletion by siRNA and small molecule inhibition

A-B) Quantification of crystal violet viability assay showing that ARID1A-KO RMG-1 (**A**) and RPE1 (**B**) cells are sensitive to siRNA knockdown of KEAP1 (mean ± SEM, one-way ANOVA, n = 3, statistically significant p-values are displayed on graph). **C-D)** ARID1A-KO RMG-1 (**C**) and RPE1 (**D**) cells grow slower than ARID1A-WT when treated with 100µM AI-1 as measured by IncuCyte S3 imaging system. Relative confluency presented as the growth from initial time point. Error bars represent SEM from 3 independent experiments. *P* values obtained from extra sum-of-squares F test on calculated logistic growth rate are indicated on graph. **E)** RPE1 ARID1A-KO cells grow slower than ARID1A-WT when treated with 10µM SFN as measured using an IncuCyte S3 imaging system. Relative confluency presented as the growth from initial time point. Error bars represent SEM from 3 independent experiments. *P* values obtained from extra sum-of-squares F test on calculated logistic growth rate are indicated on graph. **F)** ARID1A-KO CCOC cells present lower IC50 values to AI-1 than ARID1-WT cells (t-test, mean ± SEM). IC50 values were obtained from dose-response curves presented in **Supplemental Figure 2G** (n = 3).

Figure 3. ARID1A-KO cell sensitivity to KEAP1 inhibition is partly due to dysregulation of NRF2-mediated gene expression

A) Volcano plot of differentially expressed genes in ARID1A-KO RMG-1 cells from RNA-seq dataset published in Wu *et al.*[22] (blue dots if padj < 0.01, red dots if log2FC >1 or log2FC < -1 AND padj < 0.01). **B)** Top 10 enriched transcription factor target genes identified from the ARID1A-UP (*above*) and ARID1A-DOWN (*below*) regulated genes using the ENCODE[76] and ChEA[77] datasets (EnrichR[74]; $p < 0.05$ with Benjamini-Hochberg correction). **C)** Quantification of KEAP1 and ARID1A mRNA levels (RSEM, log2) from pan-cancer TCGA data (n = 10,071) showing a negative correlation between the two genes. **D)** Quantification of KEAP1 mRNA levels (RSEM, log2) from TCGA data (stomach adenocarcinoma - stad) showing higher KEAP1 levels in ARID1A-mutated patient samples (n = 90) compared to WT (n = 336) (box limits indicate 25% and 75% over median, Wilcoxon test, $p = 2.8e^{-6}$). **E)** Quantification of KEAP1 protein levels from western blot data showing higher levels in ARID1A-KO RMG-1 cells. KEAP1 intensity was normalized to respective GAPDH loading control, and then to ARID1A-WT (n = 9, mean ± SEM, t test, significant p-values displayed on graph). **F)** Quantification of crystal violet viability assay

showing that ARID1A-KO RMG-1 cells exhibit sensitivity to NRF2^{E79Q} expression induced by doxycycline (mean ± SEM, ANOVA, n = 3, significant p-values displayed on graph). **G)** Quantification of confluency (relative to DMSO control) of RMG-1 ARID1A-WT (*left*) and ARID1A-KO (*right*) cells treated with corresponding siRNAs for 48 hours, then grown in the presence or absence of AI-1 for 60 hours as measured by IncuCyte S3 imaging system (technical duplicate wells from three independent experiments; mean ± SEM, ANOVA, significant p-values displayed on graph).

Figure 4. KEAP1 inhibition exacerbates genome instability phenotypes of ARID1A-KO cells
A-B) Quantification (*left*) and representative images (*right*) of immunofluorescence experiment showing AI-1 (50μM) induces higher rates of p-RPAser33 (**A**) or γH2AX (**B**) foci formation in ARID1A-KO RMG-1 cells (mean ± SEM, ANOVA, n = 3, significant p-values displayed on graph). **C)** Representative western blot image of DNA replication stress marker p-ATR(428), p-CHK1(345), and p-RPA(ser33) in RMG-1 cells treated with siKEAP1. **D)** Quantification (*left*) and representative images (*right*) showing that ARID1A-KO RMG-1 cells accumulate higher levels of micronuclei compared to WT when treated with 50μM AI-1 (mean ± SEM, ANOVA, n = 3, significant p-values displayed on graph). White arrows highlighting micronuclei. **E)** Quantification (*left*) and representative images (*right*) showing that ARID1A-KO RMG-1 cells accumulate higher levels of micronuclei compared to WT when treated with siKEAP1 (mean ± SEM, ANOVA, n = 3, significant p-values displayed on graph). White arrows highlighting micronuclei. **F)** Quantification of confluency (relative to DMSO control) of RMG-1 cells treated with AI-1 (75μM)/ceralasertib (25nM) alone or in combination as measured after 60 hours of treatment by IncuCyte S3 imaging system (technical duplicate wells from three independent experiments; mean ± SEM, ANOVA, significant p-values displayed on graph).

Figure 5. Sensitivity of ARID1A-KO cells to KEAP1 inhibition is conserved in endometrium progenitor-derived organoid model
A) Patient-derived endometrium progenitor cell workflow. Normal endometrial tissue was processed and put in 2D culture to expand the progenitor cell population. The progenitor cells were then transduced with lentivirus containing a CRISPR sgRNA against ARID1A or a non-targeting control (NTC), and moved into 2D culture or organoid culture 24-hours later. Transducted cells were tracked using the tdTomato reporter contained in the lentiviral vector, and IHC staining for ARID1A-status was used as further validation for organoids (see **Fig S5**). Cells were treated with AI-1 at indicated concentrations and cultured for up to 10 days following the addition of the drug. **B)** Representative proliferation curves of primary endometrial epithelial cells transduced with non-targeting (NTC5) or sgARID1A (ARID1A-KO) lentivirus and treated with AI-1 at indicated concentrations as measured by IncuCyte S3 imaging system (data presented as mean of quadruplicate wells from cells derived from single patient). **C)** Representative western blot images confirming ARID1A status in NTC or sgARID1A-transduced cells. **D)** Representative western blot image of γH2AX staining showing increased DNA damage in sgARID1A-CRISPR cells after 48h treatment with AI-1. **E)** Model of ARID1A-KEAP1 synthetic lethality. Perturbation of KEAP1 dysregulates normal NRF2 signalling and proteostasis, but remains viable in normal cells. While ARID1B-containing and other BAF-

related complexes can partially compensate for ARID1A-loss, perturbation of KEAP1 in ARID1A-KO cells specifically enhances genome instability phenotypes, which is ultimately lethal.

SUPPLEMENTAL MATERIAL

Supplemental Figure 1.

A. Representative western blot images of isogenic RMG-1 ARID1A-WT and KO cells. **B-C)** Overlap of ARID1A-WT (**B**) or ARID1A-KO (**C**) fitness genes with the core essential gene training dataset (CEG2) for each replicate of our TKOv3 CRISPR screen. **D)** Representative western blot images of isogenic RPE1 ARID1A-WT and KO cells. **E)** Measurement of CRISPR editing efficiency showing single-base deletion in RPE1 ARID1A-KO clone from Sanger sequencing data using the Synthego ICE Analysis tool[70] (v3). **F)** Normalized read count data obtained using BAGEL2[72] for all four TKOv3 sgRNAs targeting KEAP1 (n=2).

Supplemental Figure 2.

A) Representative images of quantification of crystal violet staining presented in **Figure 2A-B**. **B-C)** Representative western blot showing KEAP1 siRNA knockdown efficiency in RMG-1 (**B**) and RPE1 (**C**) cells. **D)** Growth of RMG-1 ARID1A-WT and KO cells treated with increasing concentrations of SFN as measured by IncuCyte S3 imaging system. Relative confluency presented as the growth from initial time point. Error bars represent SEM from 3 independent experiments. **E)** Representative western blot image of KEAP1 and NRF2 protein levels following 24-hour treatment with AI-1 and SFN at indicated concentrations. **F)** Dose-response regression curves obtained from crystal violet survival assays for CCOC cell line panels. Confluency after 7 days of growth at indicated AI-1 concentrations was measured using crystal violet (averaged technical triplicate data from 3-4 independent experiments – or 2 independent experiments for 25µM -, mean ± SEM). IC50 values compared in **Figure 2F**. **H)** Representative western blot image of ARID1A, KEAP1 and NRF2 levels of CCOC cell line panel.

Supplemental Figure 3.

A) Quantification of KEAP1 mRNA levels (RSEM, log2) from pan-cancer TCGA data stratified by cancer subtype and ARID1A-status (significant p-values are displayed on graph). **B)** Representative western blot image showing dose-dependent induction of $NRF2^{E79Q}$ expression using doxycycline. **C)** Representative images of crystal violet staining measuring survival of cells following 7 days of dox induction. **D)** Quantification of RMG-1 ARID1A-WT and KO survival (normalized to DMSO control) showing no sensitivity to increasing concentrations of doxycycline in untransformed cells (mean ± SEM, n =3). **E)** Representative western blot image of siRNA knockdown efficiency for NRF2 and KEAP1. **F)** Representative western blot image of HDAC1 protein levels of RMG-1 cells treated with increasing concentrations of AI-1 or SFN at indicated concentrations for 24 hours.

Supplemental Figure 4.

A-B) Quantification (*left*) and representative images (*right*) of immunofluorescence experiment showing AI-1 (50µM) induces higher rates of p-RPAser33 (**A**) or γH2AX (**B**) foci formation in ARID1A-KO RPE1 cells (mean ± SEM, ANOVA, n = 3, significant p-values displayed on graph). **C-**

D) Quantification (*left*) and representative images (*right*) of immunofluorescence experiment measuring p-RPAser33 (**C**) or γH2AX (**D**) foci formation following siRNA knockdown of KEAP1 in ARID1A-KO RMG-1 cells (mean ± SEM, ANOVA, n = 4, significant p-values displayed on graph).**E-F)** Quantification (*left*) and representative images (*right*) of immunofluorescence experiment showing siRNA knockdown of KEAP1 induces higher rates of p-RPAser33 (**E**) or γH2AX (**F**) foci formation in ARID1A-KO RPE1 cells (mean ± SEM, ANOVA, n = 3, significant p-values displayed on graph). **G-H)** Quantification (*left*) and representative images (*right*) showing that ARID1A-KO RPE1 cells accumulate higher levels of micronuclei compared to WT when treated with AI-1 (**G**) or siKEAP1 (**H**) (mean ± SEM, ANOVA, n = 3, relevant p-values displayed on graph). White arrows highlighting micronuclei.

Supplemental Figure 5.
A) Representative proliferation curves of primary endometrial epithelial cells derived from two additional patients transduced (**Fig 5B**) with non-targeting (NTC5) or sgARID1A (ARID1A-KO) lentivirus and treated with AI-1 at indicated concentrations as measured by IncuCyte S3 imaging system (data presented as mean of quadruplicate wells from cells derived from a single patient). **B)** Representative IHC images of ARID1A staining for ARID1A status validation. **C)** Quantification of tdTomato+ organoids growth 10 days post AI-1 treatment at indicated concentrations (n = 1). **D)** Representative images of NTC-control and sgARID1A organoids in culture in increasing concentrations of AI-1. Arrows highlight tdTomato+ cells.

Supplemental Table 1 – CRISPR screen datasets
Sheet 1: Normalized read counts from the analysis of biological replicate 1 of our TKOv3 CRISPR screen. ***Sheet 2:*** Normalized read counts from the analysis of biological replicate 2 of our TKOv3 CRISPR screen. ***Sheet 3:*** Fold change of sgRNAs from the analysis of biological replicate 1 of our TKOv3 CRISPR screen. ***Sheet 4:*** Fold change of sgRNAs from the analysis of biological replicate 2 of our TKOv3 CRISPR screen. ***Sheet 5:*** BAGEL output of Bayes Factor, Precision, Recall and FDR values of fitness genes in ARID1A-WT and KO cells (replicate 1). ***Sheet 6:*** BAGEL output of Bayes Factor, Precision, Recall and FDR values of fitness genes in ARID1A-WT and KO cells (replicate 2). ***Sheet 7:*** Summary of all significantly enriched fitness genes identified in ARID1A-KO cells. ***Sheet 8:*** ARID1A-KO-specific hits for each biological replicate of the TKOv3 screen (i.e. synthetic lethal partners of ARID1A), along with overlap ARID1A-SL consensus from the two replicates.

Supplemental Table 2 – GO analysis (David v6.8)
Sheet 1: GO analysis of enriched biological processes for the ARID1A fitness genes identified in both CRISPR screen replicates (overlap presented in **Supplemental Table 1.7**). ***Sheet 2:*** GO analysis of enriched biological processes for the consensus ARID1A-SL dataset (103 genes, **Supplemental Table 1.8**).

Supplemental Table 3 -Differential gene expression
Differential gene expression analysis of up-regulated genes (***Sheet 1***) and down-regulated genes (***Sheet 2***) in RMG-1 ARID1A-KO cells from Wu *et al.*[22] using DESEQ2[47].

Supplemental Table 4 - Miscellaneous

Sheet 1: Reagent List. ***Sheet 2****:* p.IND20-NRF2-E79Q-HA plasmid sequence.

Supplemental Table 5 - Raw Data

Raw data for each figure presented in separate sheets.

Figure 1

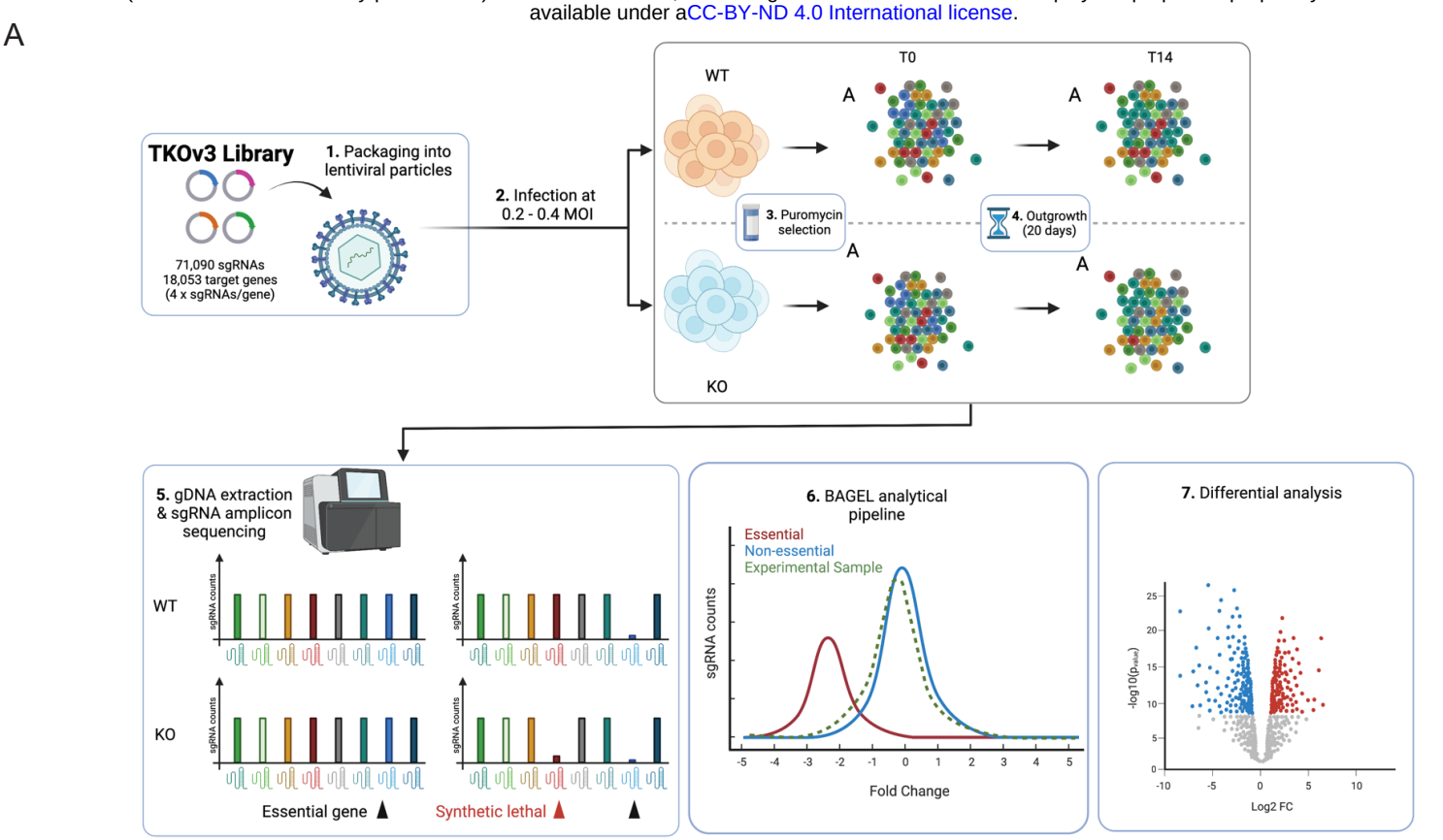

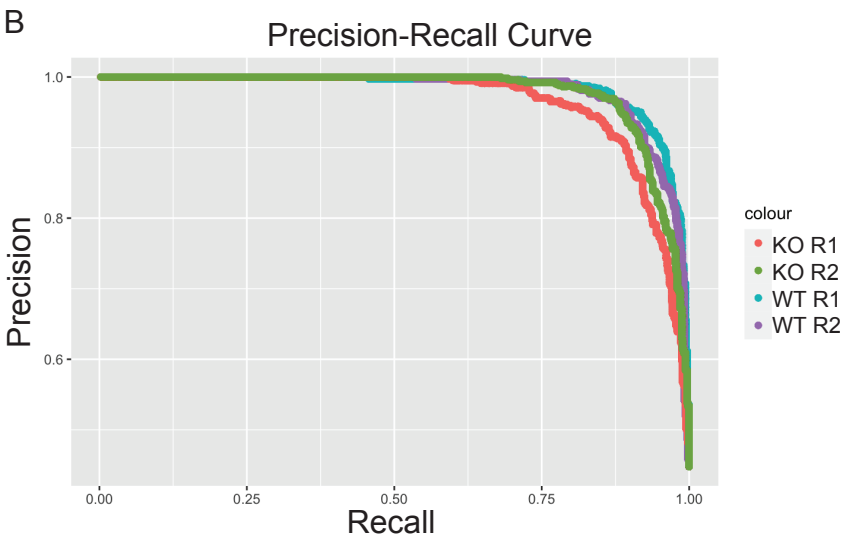

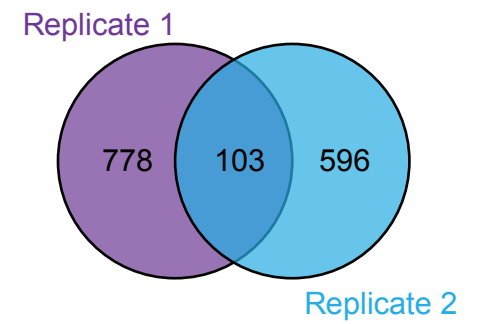

Overlap: p < 5.588e-26, hypergeometric test

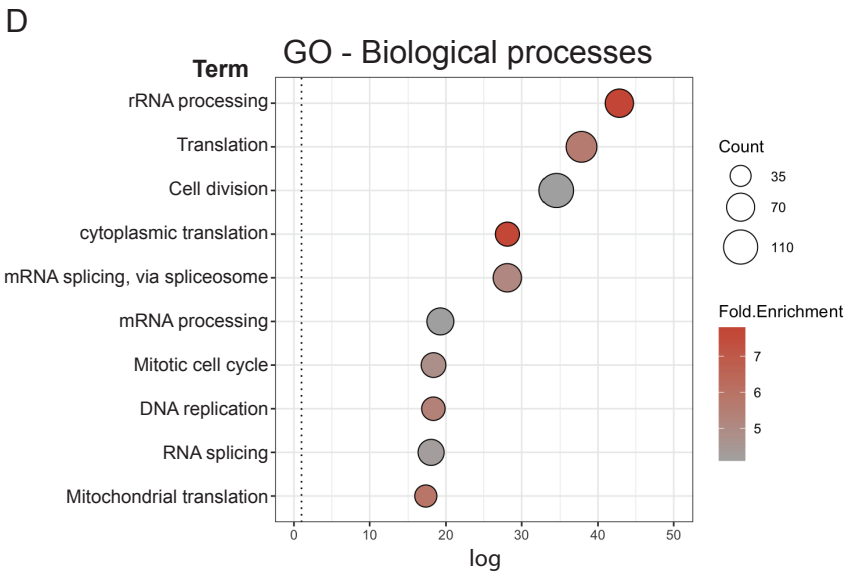

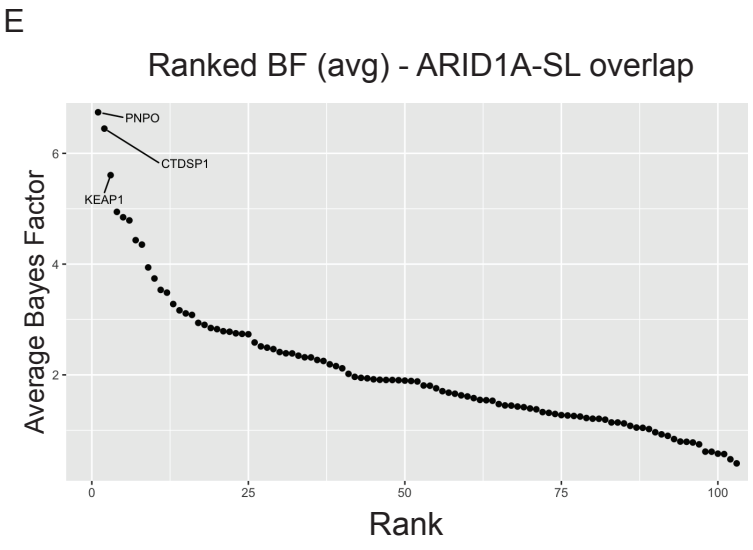

Figure 2.

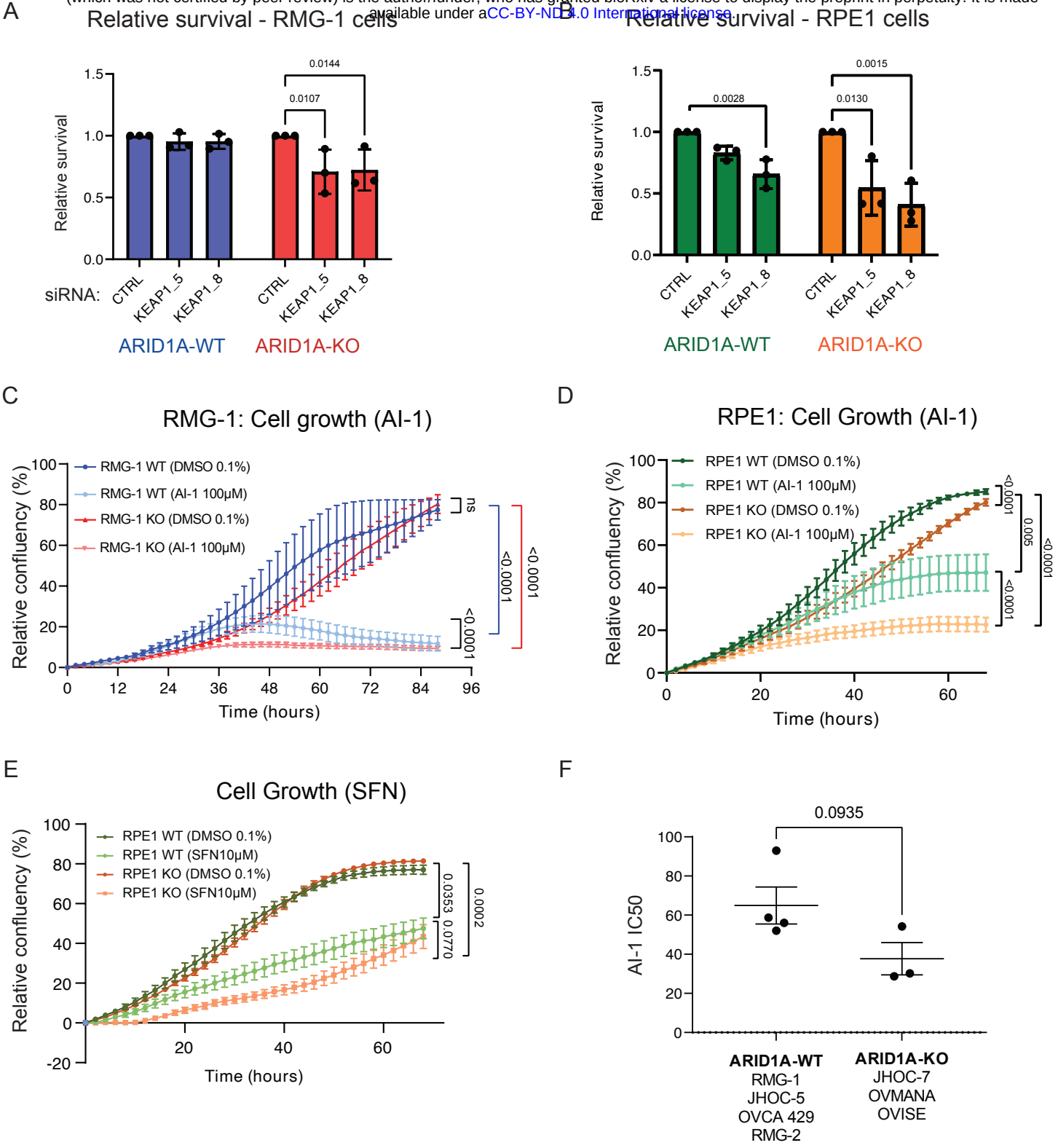

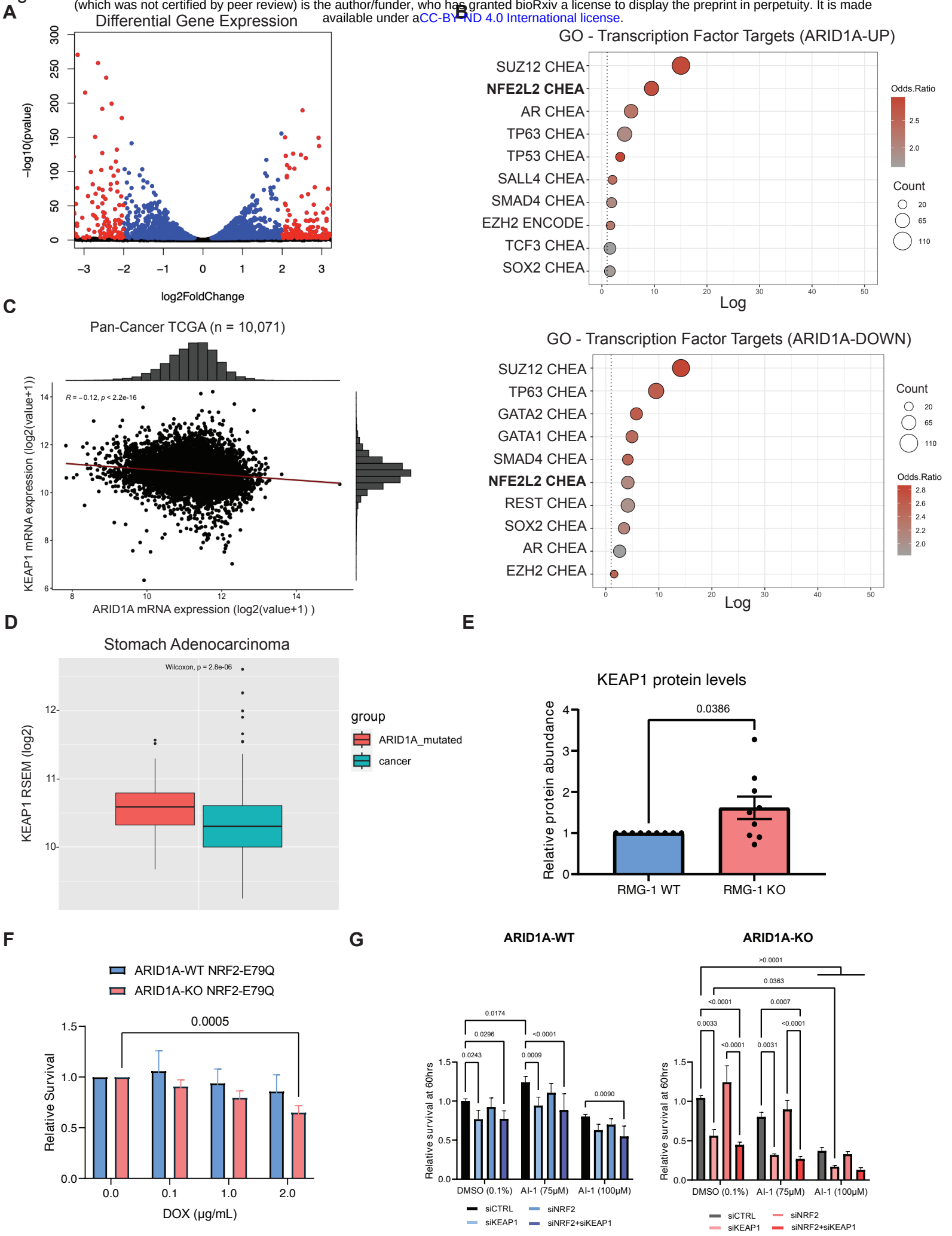

Figure 4

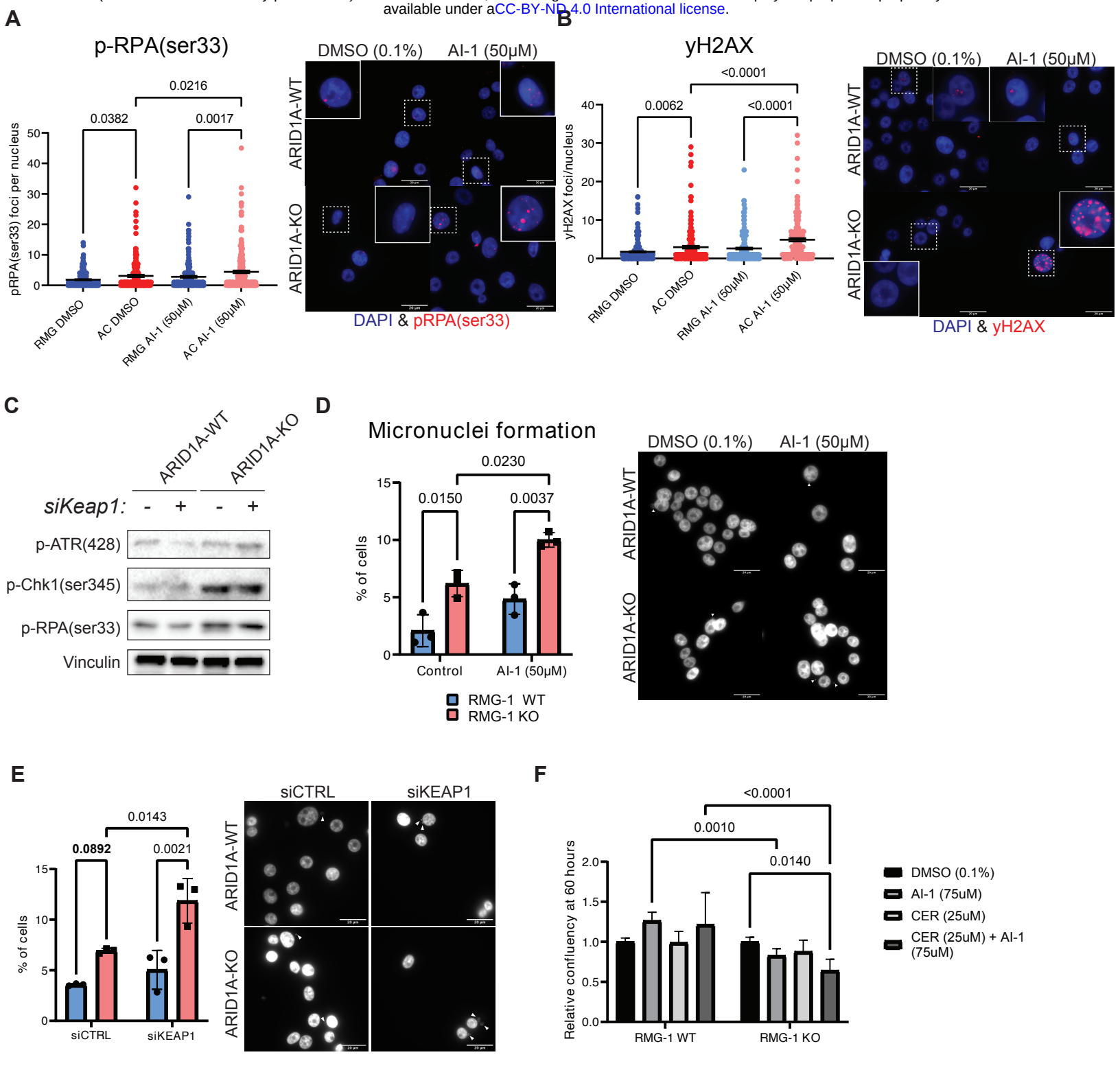

Figure 5.

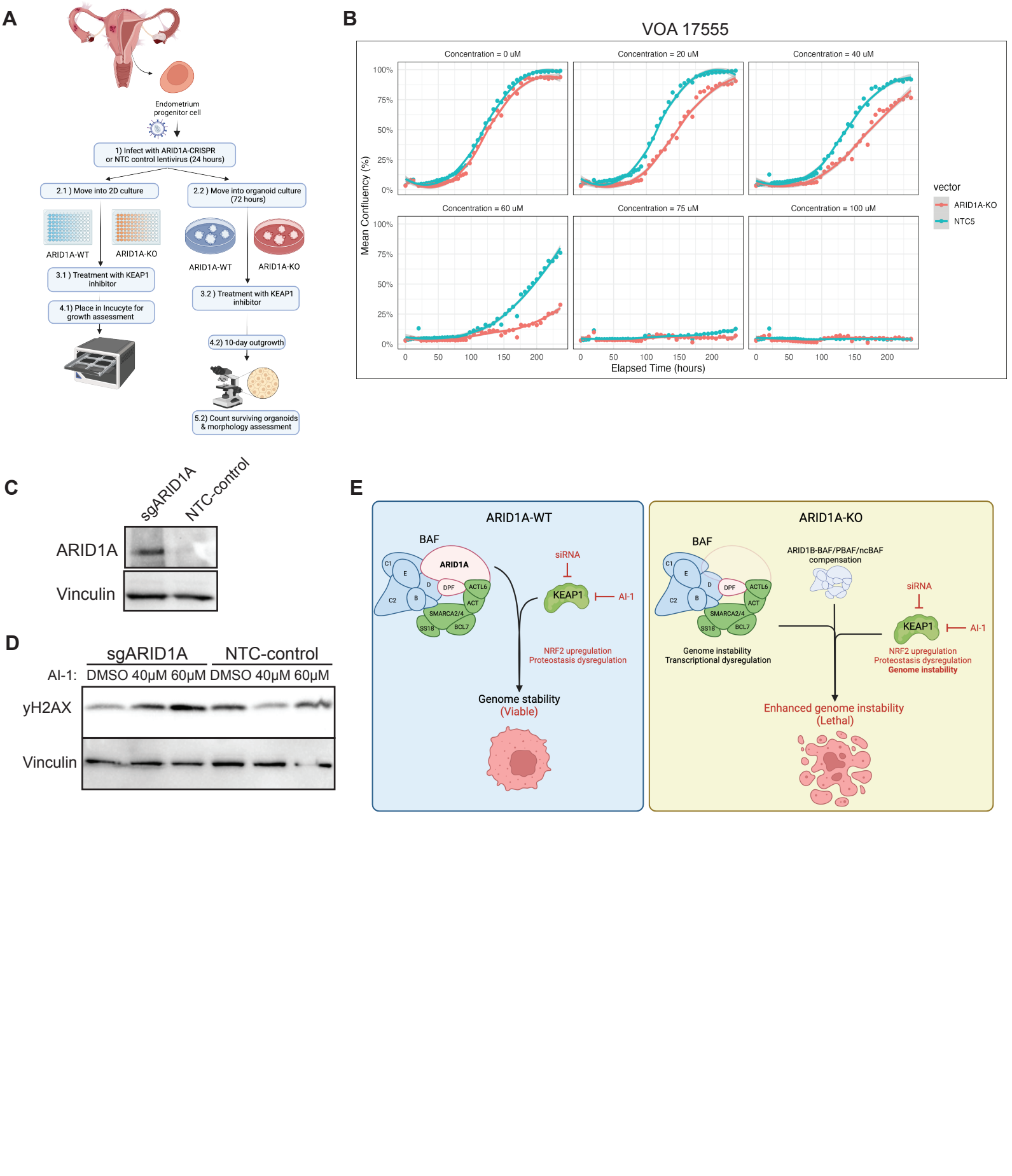

Supplemental Figure 1

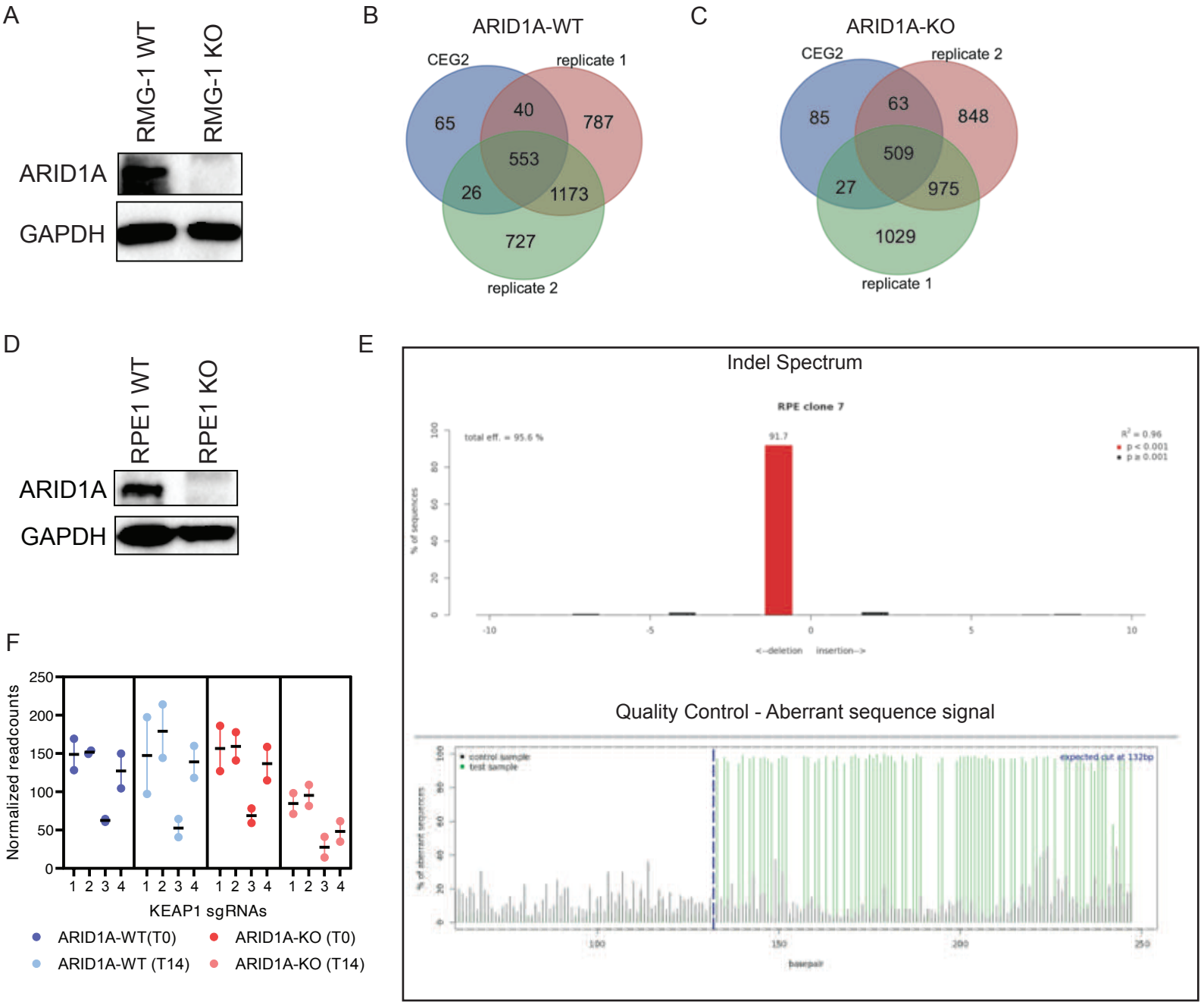

Supplemental Figure 2

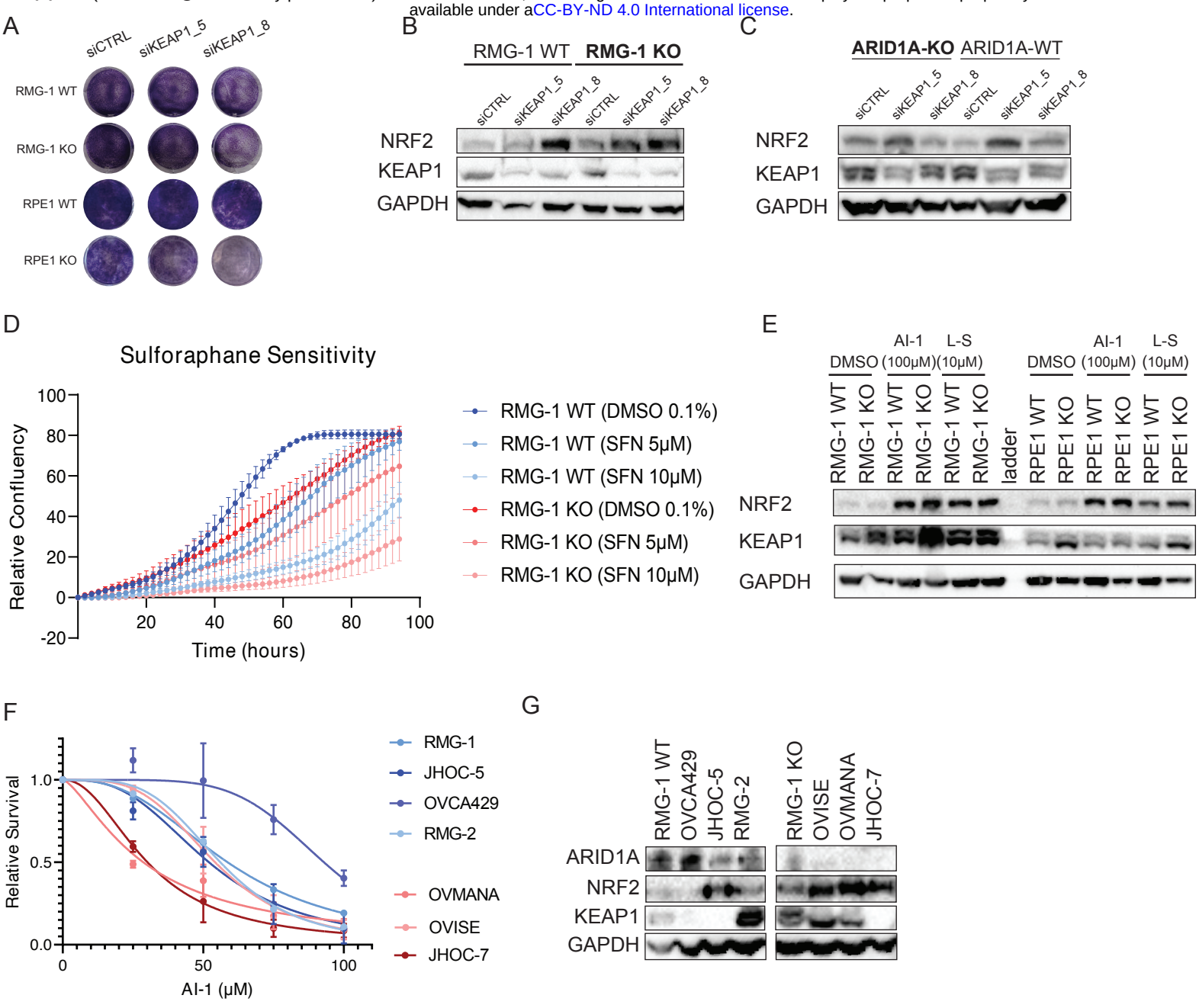

A

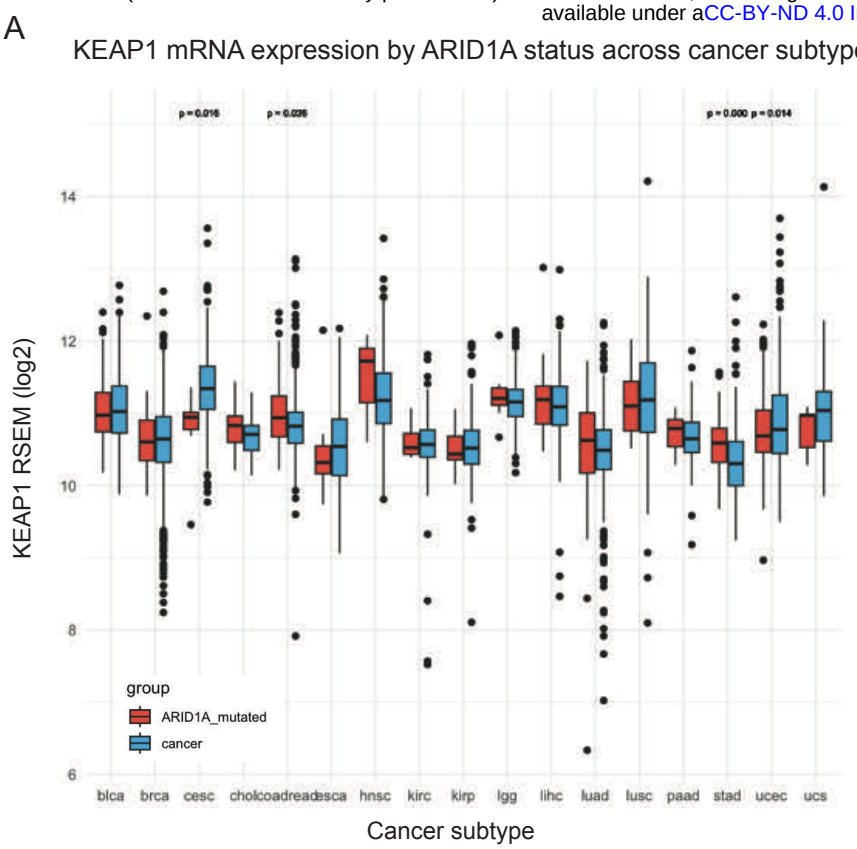

B

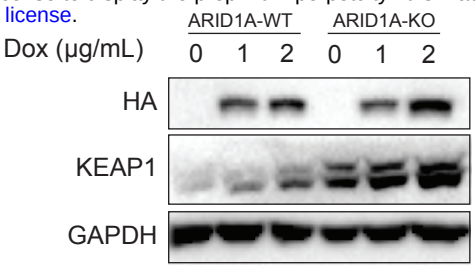

C

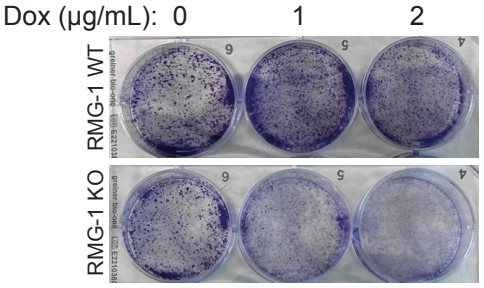

D

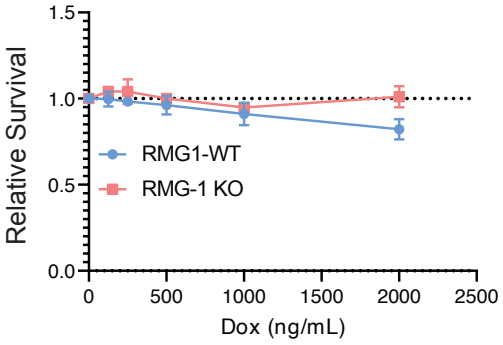

E

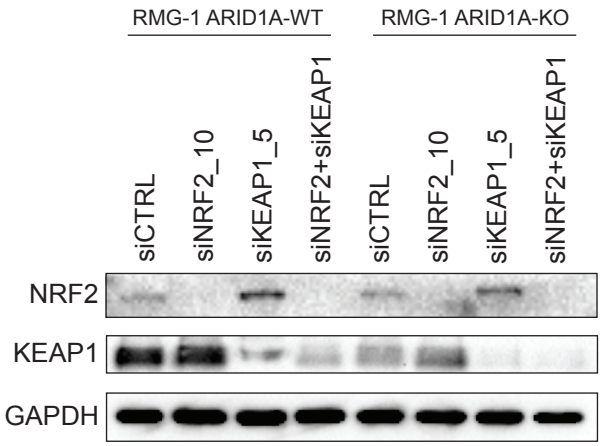

F

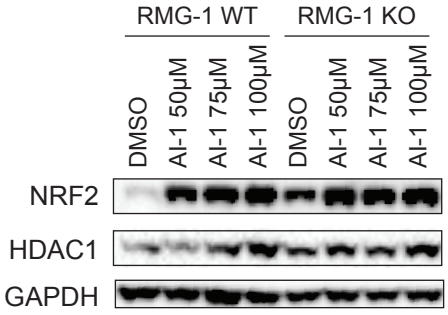

Supplemental Figure 4

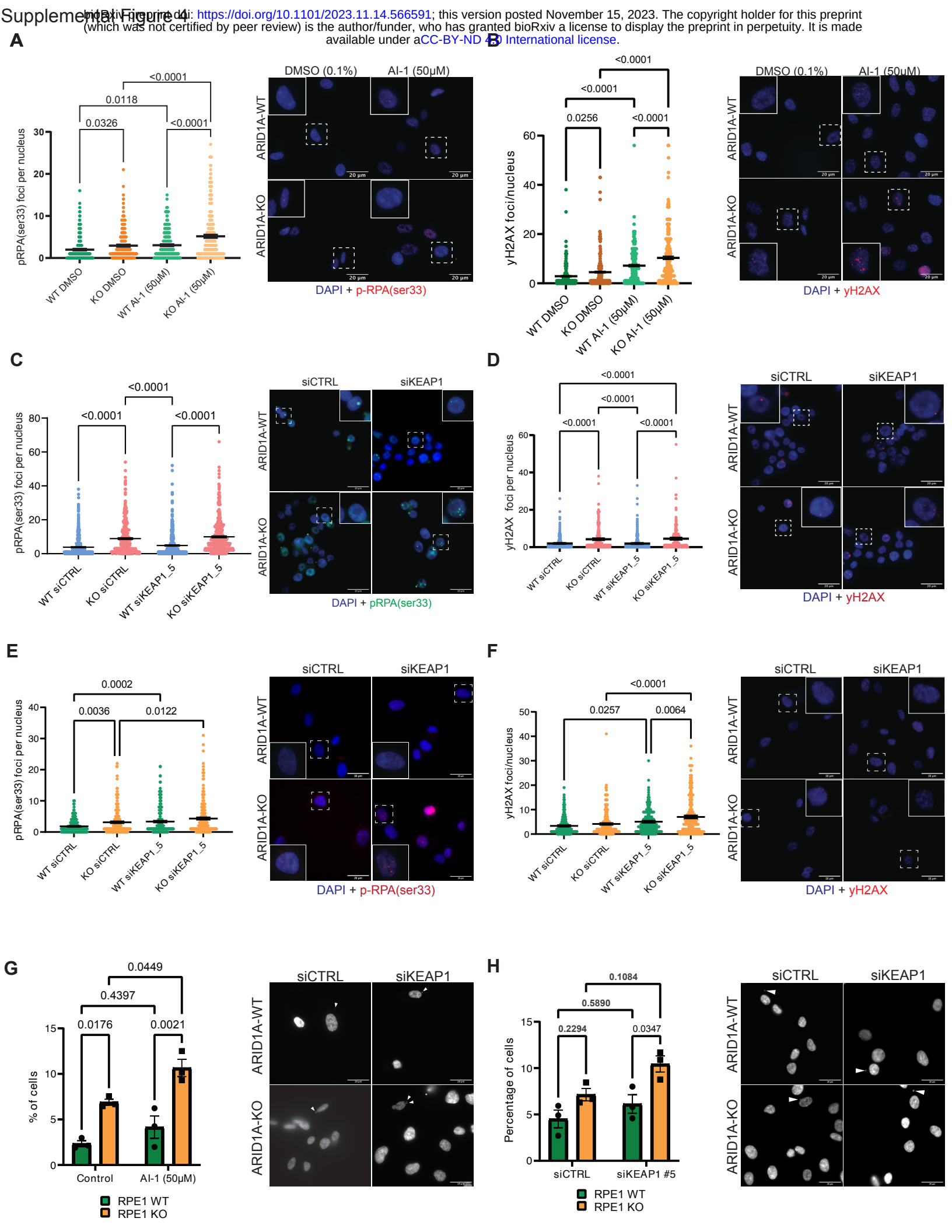

Supplemental Figure 5